International Journal of Applied Pharmaceutics

ISSN- 0975-7058 Vol 18, Issue 3, 2026

Original Article

DUAL-LOADED PHYTOSOMES OF PAPAIN AND ALOE VERA: FORMULATION AND EVALUATION OF DIABETIC WOUND HEALING PROPERTIES

SAJISHA VS, ASWIN VISWANATH, SAURABH SINGH*, SHEETU WADHWA

School of Pharmaceutical Sciences, Lovely Professional University, Punjab-144411, India
***Corresponding author: Saurabh Singh; *Email: saurabh.baghel1214@gmail.com**

Received: 07 Dec 2025, Revised and Accepted: 14 Mar 2026

ABSTRACT

Objective: The goal of this study was to prepare and evaluate phytosomes containing *Aloe vera* extract and papain using the solvent evaporation method.

Methods: We prepared phytosomes of *aloe vera* extract and papain by the solvent evaporation technique. Design-Expert® software (version 11.0.5) was used for the optimisation procedure. Out of 17 formulations, F8 was selected as the best, on the basis of particle size, polydispersity index (PDI), and entrapment efficiency (EE). Mixing the best formulation (F8) with carbopol 940, a phytosomal gel was prepared for better compliance. The gel was tested for its physicochemical properties, antioxidant properties by DPPH assay, cytotoxicity by MTT assay, and α-amylase inhibitory activity as an indicator of antidiabetic potential**.** *In vivo* diabetic wound healing was tested on streptozotocin (STZ)-induced wistar rats for 25 d.

Results: The optimised formulation (F8) had a particle size of 87.3±0.05 nm, a polydispersity index of 0.30±0.001, and a zeta potential of −55.6 mV, indicating high colloidal stability due to electrostatic repulsion. The entrapment efficiency of F8 for papain was 95.62±0.01% and 96.35±0.01% for aloe vera extract. pH 6.4±0.05, viscosity 20.11±0.00057 Pa·s, and spreadability 21.72±0.58 g·cm/s of the gel formulation were considered in the acceptable range. The SEM analysis verified a consistent and distinct vesicular morphology. The formulation showed strong antioxidant activity (IC_{50} = 35.3 µg/ml), 85.71% cell viability, and moderate α-amylase inhibition (56±9.19%) without implying systemic glycaemic control. *In vivo* studies showed that the higher the dose, the faster the wound healed. By day 17, the high-dose group had 92.09±1.77% wound contraction, and by day 25, the wound was completely closed (100%), which was much better than the control group ($p<0.05$).

Conclusion: The active ingredients were successfully shielded from oxidation and degradation by encapsulating papain and *aloe vera* polysaccharides in lipid-based phytosomes. This delivery system offers a promising therapeutic strategy for treating diabetic wounds and oxidative stress.

Keywords: *Aloe vera*, Drug delivery, Diabetes, Oxidative stress, Papain, Phytosome, Wound healing

DOI: https://dx.doi.org/10.22159/ijap.2026v18i3.57725 Journal homepage: https://innovareacademics.in/journals/index.php/ijap

INTRODUCTION

Bioactive phytocompounds from diverse sections of medicinal plants have been used since ancient times to treat various diseases. Today, they are globally recognised as important agents of disease prevention. Phytocompounds extracted or isolated from different plant sections offer numerous therapeutic benefits [1]. However, their clinical applications are often limited by poor solubility, low permeability, and reduced bioavailability. According to the world health organization (WHO), plant-based medicines continue to be used as safe and non-toxic complementary treatments, especially in developing countries, despite advancements in conventional therapies [2]. Despite their promising therapeutic potential, physicochemical limitations often hinder the clinical translation of phytocompounds, such as poor aqueous solubility, low gastrointestinal permeability, rapid metabolism, and insufficient systemic bioavailability [3]. These challenges significantly reduce their therapeutic efficacy and restrict their use in conventional dosage forms overcome these limitations, novel drug delivery systems have emerged as promising strategies for enhancing the bioavailability and therapeutic effectiveness of phytoconstituents [4]. Among these, nanotechnology-based carriers, such as phytosomes, liposomes, nanoemulsions, and polymeric nanoparticles, have demonstrated the ability to improve solubility, protect bioactives from degradation, and promote targeted delivery. Among these systems, phytosomes stand out as particularly promising and versatile carriers for enhancing the bioavailability, therapeutic efficacy, and targeted delivery of phytoconstituents [5]. Owing to their unique structural resemblance to biological membranes, phytosomes enable close interactions with physiological systems, thereby improving the pharmacokinetic profile of encapsulated compounds [6]. These vesicular structures can significantly enhance the oral bioavailability of polar phytoconstituents by increasing their cellular absorption and reducing the required therapeutic dose [7]. Among the plant-derived compounds that can significantly benefit from such advanced delivery systems are those found in *aloe vera* and papain, which are known for their distinct therapeutic benefits.

Aloe vera is a fleshy perennial plant from the A*sphodelaceae* family that has been known for a long time to have healing properties and is used a lot to treat many human illnesses [8]. People know that this plant can be used for medicine, cosmetics, and nutrition. *Aloe vera* extracts contain bioactive compounds with unique molecular structures, such as aloesone, aloesin, aloin, and aloe emodin. These compounds may be used in nanotechnology-driven medicine, and they are getting more and more attention in advanced formulation studies [9, 10]. People know that these bioactive compounds can affect many bodily functions, and there is more and more proof that they help keep blood sugar levels stable, especially by changing how the liver processes glucose. This makes *aloe vera* a good choice for managing diabetes [11]. *Aloe vera* gel extract has been shown to lower fasting blood sugar levels, boost insulin production, and help pancreatic islet cells recover both structurally and functionally [12]. These results show that *aloe vera* could be used to treat diabetes and show that more research is needed to find the specific biomolecules that cause these effects [13]. It is thought that *aloe vera* gel helps drugs move across the intestinal epithelium by making epithelial tight junctions open and close again [14]. So, giving *aloe vera* products along with medicines that are slowly absorbed makes the compound more available to the body [15]. Phytosomal processing changes phytoconstituents into lipid-soluble parts because *aloe vera* extract can also dissolve in water [16].

Papain [EC 3.4.22.2], a cysteine protease with a molecular weight of 23,406 kDa, consists of a 212 amino acid polypeptide sequence [17]. It is found in papaya (*Carica papaya*) and mountain papaya (*Vasconcellea cundinamarcensis*), which aid in infection and wound healing [18]. An increase in the

quantity of papain-like cysteine proteases in plants correlates with an increased ability of plants to survive various types of stress [19]. Papain is more prevalent in unripe fruits and is listed as a generally recognised as safe (GRAS) enzyme by the US food and drug administration (FDA) [20]. As per previous studies, papain boosts tissue growth and antimicrobial activity when applied to the wound area [21]. It also enhances the liquefaction of purulent discharge, activates tissue regeneration, and minimizes healing time [22]. Despite its strong proteolytic activity, papain is safe for use on wound surfaces due to its specificity for dead tissue. This enzyme can accelerate tissue regeneration, making papain a potential treatment option [23].

Papain and *aloe vera* have complementary and synergistic effects on diabetic wound healing, by simultaneously targeting the main pathological barriers associated with diabetic wounds. Papain, a proteolytic enzyme, facilitates efficient enzymatic removal by selectively breaking down necrotising tissue, fibrin deposits, and devitalized proteins, thereby promoting a cleaner wound surface and allowing more rapid progression to the proliferative stage [24]. Varieties of chemicals in *aloe vera,* such as acemannan, vitamins (A, C, E, and B-complex), minerals, amino acids, phenolic compounds, anthraquinones, enzymes, and plant sterols, which together provide antioxidant, anti-inflammatory, antimicrobial, and pro-regenerative effects [25]. *Aloe vera* extract stimulates collagen synthesis, angiogenesis, fibroblast proliferation, and cytokine signaling, which are critical for diabetic wound repair. It is thought to bind to M-type phospholipase A2 receptor and induce an intracellular signalling pathway [26]. The *aloe vera* polysaccharide also stabilises papain and protects the enzyme from oxidative degradation and excessive protease activity in the chronic wound microenvironment, thereby prolonging its therapeutic effect [27].

To the best of our knowledge, this is the first report on the development of dual-loaded phytosomes co-encapsulating papain and Aloe vera, designed to synergistically combine enzymatic debridement and phytochemical-mediated wound healing within a single lipid-based nanocarrier.

MATERIALS AND METHODS

Materials and reagents

Aloe vera was collected from the malabar botanical garden, kozhikode, kerala, and authenticated by Mr. Harinarayanan C M, scientist, pharmacognosy division, kottakkal arya vaidya sala, kerala. The plant specimen was assigned the voucher number CMPR/AIF/PHG/224 and stored in the pharmacognosy division of the kottakkal arya vaidya sala in kerala. Papain (TC 685), streptozotocin (STZ) (S0130) of purity ≥ 98% and phosphatidylcholine (PC) (P5638) of purity ≥ 95%, 2,2-diphenyl-1-picrylhydrazyl (DPPH), and 3-(4,5-dimethylthiazol-2-yl)-2,5-diphenyltetrazolium bromide (MTT) reagent were purchased from sigma-aldrich. Carbopol 940, fehling's solution, ferric chloride, glacial acetic acid, hager's reagent, hydrochloric acid, lead acetate solution, and triethanolamine were purchased from loba chemie pvt. ltd, lead standard (Pb), mercury standard (Hg), and propylene glycol from merck india. Haematoxylin and eosin was purchased from himedia laboratories. All the other reagents and chemicals used were of analytical grade.

Methods

Preparation of aqueous extract of *aloe vera*

Aqueous *aloe vera* extract was prepared by weighing 250 g of *aloe vera* gel collected from fresh, thoroughly washed *aloe vera* leaves. The weighed amount of gel was washed with deionised water to remove latex and other dissolved impurities, before subsequent grinding to a solution [28].

Phytochemical analysis

Phytochemical analysis of the *aloe vera* extract was performed to determine the presence or absence of major classes of secondary metabolites. The list comprised steroids, phenols, alkaloids, flavonoids, coumarins, saponins, tannins, phlobatannins, glycosides, anthraquinones, carbohydrates, proteins, and terpenoids [29]. The procedures implemented were adapted from established protocols, as referenced in the literature and related sources.

Drug excipient compatibility study

A study was conducted to evaluate the compatibility of drug excipients using fourier-transform infrared (FTIR) spectroscopy. FTIR spectra were obtained for the drug, the excipient, and their physical mixture to identify potential interactions by analysing the spectral peaks. Approximately 1 mg of the sample and 100 mg of potassium bromide were combined in a mortar and ground into a fine powder using a pestle. A small portion of the triturated sample was placed in a pellet maker and compressed at a pressure of 10 kg/cm^2. The resulting pellet was positioned in the sample holder and scanned over a range of 3600–300 cm^{-1}. Significant peaks have been documented [30].

Optimisation of formulation variables

The experimental design for optimising dual phytosomes was conducted using design expert software version 11.0.5. A box–behnken design (BBD) was utilised to assess the impact of three independent variables: concentrations of *aloe vera* and papain (mg), and phospholipid concentration (mg), on three critical responses: particle size (nm), PDI, and entrapment efficiency (E E %). The experimental setup proposed 17 trials, leading to the development and characterisation of 17 prototypes (F1 to F17) for particle size as Y1, and the entrapment efficiency of *aloe vera* extract and papain as Y2 and Y3, with PDI as Y4 serving as response parameters. The responses from these 17 trials (F1–F17) were analysed using various statistical models. Among all the batches (F1 to F17), batch F8 exhibited the smallest particle size (Y1), the highest entrapment efficiency (Y2 and Y3), and the lowest PDI (Y4), making it the preferred choice for further validation. The polynomial equations derived for responses Y1, Y2, Y3, and Y4 facilitated the creation of 2D and 3D response surface plots and perturbation plots for particle size, % entrapment efficiency, and PDI [31].

Model significance and adequacy

Analysis of variance (ANOVA) was performed to evaluate the statistical significance of the fitted quadratic models for all four responses: particle size, papain entrapment efficiency (EE-P), *aloe vera* extract entrapment efficiency (EE-A), and PDI [32].

Preparation of *aloe vera*–papain phytosomes by the solvent evaporation method

Phytosomal complexes of *aloe vera* extract and papain were created using the solvent-evaporation method. A specific amount of phospholipid was fully dissolved in 6 ml of dichloromethane in a clean, dry round-bottom flask with gentle stirring. Simultaneously, exact quantities of *aloe vera* extract and papain were measured and dissolved in 4 ml of phosphate buffer at pH 7.0 to create a uniform aqueous solution. The *aloe vera*–papain solution was then slowly and separately added to a round-bottom flask containing the phospholipid–dichloromethane (DCM) mixture, with continuous stirring to aid in the formation of a pre-complex emulsion at the interface of the organic and aqueous phases. The flask was then attached to a rotary evaporator (RV 8599, IKA India pvt. ltd), and the organic solvent was removed under reduced pressure at temperatures not

exceeding 40 °C, resulting in a uniform thin lipid film containing the drug-phospholipid complex. The dry film was rehydrated with phosphate buffer, and the resulting dispersion was sonicated to reduce particle size [33]. All formulations (F1–F17) were prepared using this same method.

Physicochemical characterization of phytosomes

The average size distribution of phytosomes is a crucial parameter that affects the overall performance of the product. Particle size is a crucial factor in determining the drug absorption and distribution. The amounts of phytoconstituents and phospholipids required to prepare stable phytosomes were optimized by preparing different batches.

Zeta potential and particle size

Particle size is an important factor in drug absorption and distribution. Particle size analysis was performed using a "malvern zeta sizer nano ZS (malvern instruments, UK)" based on dynamic light scattering principles. The samples were diluted in distilled water (1:200) and placed in disposable plastic cuvettes [34].

Entrapment efficiency (%)

The entrapment efficiency of the phytosomes was assessed by centrifugation. Vesicles were isolated using a high-speed cooling centrifuge (REMI ultra-centrifugation) at 10,000 rpm for 30 min, with the temperature maintained at 37 °C. The concentration of the free drug was determined from the supernatant (10 ml) collected after centrifugation. The absorbance of papain and aloe vera extract was measured at 220 and 211 nm, respectively, using a UV spectrophotometer (shimadzu, japan). Subsequently, the entrapment efficiency was calculated using the following equation [33].

$$\% \square \square = \frac{\square\square\square\square\square\ \square\square\square\square\square\square\ \square\square\ \square\square\square\square\ - \square\square\square\square\square\square\ \square\square\ \square\square\square\square\ \square\square\square\square}{\square\square\square\square\square\ \square\square\square\square\square\square\ \square\square\ \square\square\square\ \square\square\square\square} \times 100$$

Preparation of phytosomal gel

The gel base was formulated using carbopol 940 and distilled water, with the water quantity being approximately 20 times the weight of carbopol 940. The mixture was allowed to rest for approximately 20 min before stirring. Subsequently, triethanolamine, a neutralising agent, was introduced into the gel base. Following the formation of the gel base, the phytosome suspension was incorporated and stirred until a homogeneous gel consistency was achieved. Finally, methylparaben was dissolved in a portion of propylene glycol, and vanilla essence was added and thoroughly mixed [34].

Organoleptic observation

Organoleptic evaluation was conducted by examining the texture of the formulation and any alterations in the colour and odour of the gel. These observations were performed on both freshly prepared and stored gel samples. Stable gels should maintain consistent characteristics in terms of colour and odour before and after exposure to accelerated storage conditions [35].

P^{H}

The pH meter was calibrated using standard buffer solutions of pH 4 and 7, respectively. Approximately 0.5 g of gel was weighed, dissolved in 50.0 ml of distilled water, and its pH was measured.

Viscosity

The viscosity of the formulation was determined using a brookfield viscometer (model no. LVDV-E viscometer) at 100 rpm using spindle no. 7 [36].

Spreadability

Two glass slides (0.2 m × 0.2 m) were used. A small amount of the sample was sandwiched between two glass slides. A 1 g weight was placed on the upper slide to uniformly press the gel between the two slides and form a thin layer. The weight was removed and fixed to a stand without the slightest disturbance, so that the upper slide slid off freely under the force of the weight tied to it. The time taken for the upper slide to separate from the lower slide was measured using a stopwatch. Subsequently, the average diameter was determined. This procedure was repeated by successively adding the other slides at one-minute intervals. The parallel plate method is the most widely used method for determining and quantifying the spreadability of semisolid formulations. The following equation was used for this purpose [37].

$$\text{Spreadability, S} = \frac{d^2\Pi}{4}$$

Drug content

To determine the drug content, 1 g of the prepared gel was accurately weighed, dissolved in 10 ml of ethanol, and filtered. A 1 ml aliquot of the filtrate was diluted to 100 ml with a pH 7.4 buffer and analysed using a UV spectrophotometer (shimadzu, japan) at 220 and 211 nm [38].

Porability

A measuring cylinder was filled with a freshly homogenized formulation. After standing for 30 min, the test sample was poured according to a standardized pouring procedure, and the amount remaining in the cylinder was determined. If required, the cylinder may be rinsed up to three times with water, and the amount remaining in the cylinder after each rinsing step is determined [39].

The residue (R) of the pourability was calculated using the following equation

$$R = \left[\frac{m_2 - m_0}{m_1 - m_0}\right] \times 100$$

$$\mathbf{R'(n) = \frac{m'n - m_0}{m_1 - m_0} \times 100}$$

Homogeneity

The developed gels were evaluated for uniformity through visual inspection after placement in containers. The assessment focused on their appearance and the presence of aggregates. Additionally, the formulations were checked for homogeneity based on their visual appearance [40].

Particle size and PDI

Particle size analysis was performed using a "malvern zeta sizer nano ZS (malvern instruments, UK)" based on dynamic light scattering principles [41].

Differential scanning calorimeter (DSC) analysis

The thermogram of the phytosome was recorded using a DSC (shimadzu DSC-60, japan) and aluminium pans. Dry phytosome samples (weighing between 2.00 and 10.00±5 mg) were individually measured, placed in sealed aluminium pans, and heated at a rate of 10 °C per minute over a temperature range of 30–300 °C. A purifying nitrogen stream was maintained at a flow rate of 40 ml/min to create optimal conditions [30].

DPPH radical scavenging activity

The DPPH assay is a commonly used method to evaluate the antioxidant activity of a compound, extract, or formulation. When an antioxidant donates a hydrogen atom or electron to DPPH, it is reduced, and the colour changes to yellow. The intensity of this colour change is proportional to the scavenging ability of the antioxidant, which can be measured spectrophotometrically. The DPPH test was used to estimate the antioxidant properties of the *aloe vera* extract, papain, and phytosomes containing *aloe vera* extract and papain. The free radical scavenging activity of the sample was estimated by preparing a methanolic solution of DPPH. Various concentrations of the sample (10-80 µg/ml) were added to DPPH solutions in a 1:1 ratio. The samples were placed in a dark area. Ascorbic acid was used as a standard for comparison [43].

$$\% \textbf{ inhibition } = \textbf{ A0} - \textbf{A/A0 } \times \textbf{ 100}$$

A_0 = Absorbance of DPPH in the absence of the sample

A = Absorbance of DPPH in the presence of the sample

Determination of IC 50

The IC_{50} values for the *aloe vera* extract, papain, phytosome, and the standard antioxidant, ascorbic acid, were determined by plotting the concentrations on the x-axis against the corresponding percentage inhibition of DPPH radicals on the y-axis. The data were analysed using microsoft excel to generate inhibition curves and calculate IC_{50} values [43].

α-amylase activity

The α-amylase-inhibiting power of the phytosome was quantified by measuring the reducing sugar, maltose, under specified conditions. To estimate the maltose equivalent, a modified dinitro salicylic acid (DNS) method was used. Here, 1 ml of the phytosomal suspension was preincubated with α-amylase enzyme (1U) for 30 min. Subsequently, a 1% (w/v) starch solution (1 ml) was added to the mixture and incubated for 10 min at 37 °C. DNS reagent (1 ml of DNS reagent was added to the sample solution as a reaction stopper and heated for 5 min in a water bath, and the absorbance was measured at 540 nm. Acarbose (100µg/ml) served as a positive control, and the buffer solution served as a blank [44, 45].

Statistical analysis

Statistical analyses were performed using graph pad prism 10.3. As there were two factors, a two-way analysis of variance (ANOVA) was applied, followed by tukey's post-hoc test.

MTT assay

This colourimetric assay quantifies mitochondrial activity as an indicator of cytotoxicity and viability. Normal human dermal fibroblasts (NHDF) were cultured in RPMI-1640 medium (sigma-aldrich, USA) supplemented with 10% fetal bovine serum (FBS), 1% antibiotic-antimycotic solution, 0.01M HEPES, 0.02 mg/ml-glutamine, and 0.001 M sodium pyruvate to support optimal cell growth. The cells were maintained in a humidified incubator at 37 °C with 5% CO_2. Cell viability was determined from the optical density measured at 570 nm. Povidone iodine is used as a standard [47, 48]. The untreated cell served as a blank.

$$\text{Cell viability (\%)} = \frac{\text{Optical density (OD)of sample}}{\text{Optical density (OD) of control}} \times 100$$

Statistical analysis

Statistical analyses were performed using graph pad prism 10.3. One-way analysis of variance (ANOVA) was performed, followed by tukey's multiple comparison test.

Stability studies

Stability was evaluated by assessing changes in particle size, drug entrapment efficiency, and physical appearance over six-months. The entire sample was kept for six months in an air tight amber coloured bottle at 25 °C/65% RH and 40 °C/75% RH. At consistent intervals of zero, one, three, and six months, the samples were drawn and analysed for any considerable change in particle size, entrapment efficiency, and physical appearance [49].

Diabetic wound healing activity

Animals were procured from the in-house animal housing facility. After the veterinary examination, the rats were acclimatised for seven days before treatment. The animals were divided into four groups, each containing six animals. The sample size (n = 6 per group) was selected based on a prior STZ-induced diabetic wound-healing model. A minimum of six animals per group was sufficient to provide adequate statistical power (≥80%). The animals were randomly allocated to the treatment groups using a random number-based allocation method. This study did not implement blinding for outcome assessment, which is recognised as a drawback; however, standardised evaluation criteria were consistently implemented across all groups to mitigate observational bias.

On day 0, the animals were anaesthetized, the fur on the dorsum of each animal was shaved, and a wound area was created on the dorsal interscapular region 5 mm away from the ears using a circular-coloured rubber stamp. Full-thickness skin from the demarcated area, including the panniculus carnosus, was excised to obtain a wound area of approximately 500 mm^2. Except for Group I, all groups received the assigned treatment until complete wound closure was achieved. Body weights were monitored on days 0,1,7, 14, 21, and 28. The wound area was measured on alternate days until complete epithelialization (i. e., days 0,1,5,9,13,17, 21, and 25). The percentage of wound closure was calculated [50]. Statistical

analyses were performed using the graphpad prism 9 software. Two-way ANOVA and tukey's multiple comparison tests were used. Statistical significance was set at P<0.05. The experimental protocol was approved by the IAEC, having IAEC approval number: JSSCP/OT/IAEC/13/2025-26).

Induction of diabetes

After overnight fasting, the animals were intraperitoneally injected with a freshly prepared solution of STZ (35 mg/kg) in a citrate buffer. The development of hyperglycaemia in these rats was confirmed by measuring their fasting blood glucose levels 3 d after STZ injection. Animals with fasting blood glucose levels>250 mg/dl were considered diabetic and included in the study [51].

Parameters to be observed

Body weight

The body weights of the animals will be determined on day 0,1,7,14, 21, and 28.

Wound area and percentage wound closure

The physical attributes of wound healing, such as wound area and percentage wound closure, were studied by tracing raw wounds. The wound area was measured by tracing the wound on days 0,1,5,9,13,17,21, and 25. The percentage of wound closure was calculated using the following formula [50].

$$\% \text{ wound closure } = {\text{Wound area on day 0} - \text{Wound area on day N}}/{\text{Wound area on day 0}}$$

Where N = Wound area on the corresponding days

Histopathological analysis

At the end of the study, the wound tissues were collected and fixed in 10% formalin for histological analysis. After removing lipid debris by soaking in alcohol, the sections were dehydrated using increasing ethanol concentrations, and the tissue samples were embedded in paraffin wax. The section, which is a 5-10 µm-thick coronal section of wound tissue with a thickness of 2 mm, was taken using a microtome. The slides were stained with haematoxylin and eosin (H and E). The stained tissue sections were observed under a microscope (40x), and the wound tissue region was photographed to assess the changes observed with different treatments [51].

RESULT AND DISCUSSION

Phytochemical analysis

Table 1: Results of the phytochemical screening of *aloe vera* extract

S. No.	Phytoconstituents	Presence/absence
1	Alkaloids	+
2	Flavonoids	+
3	Sterols	+
4	Saponin glycosides	+
6	Tannins	+
7	Cardiac glycosides	-
8	Anthraquinones	+
9	Balsams	-
10	Volatile oils	-
11	Steroids	-

Key: (+) indicates the presence of compound and (-) indicate the absence of compound.

Drug-excipient compatibility

FTIR spectra of the drug, excipient, and phytosome were obtained as shown in fig. 1-3. The FTIR spectrum of the formulation (fig. 3) revealed characteristic peaks, confirming the formation of a phytosomal complex between papain, *aloe vera* extract, and phospholipids. The prominent absorption bands observed at 2916.37 cm^{-1} and 2848.93 cm^{-1} correspond to the asymmetric and symmetric stretching vibrations of aliphatic C–H groups, respectively, indicating the presence of phospholipid chains. A strong band at 1705.07 cm^{-1} represents the C=O stretching vibration of carbonyl groups, suggesting ester or amide linkages, while the absorption at 1573.91 cm^{-1} is attributed to N–H bending and C–N stretching of amide II, confirming the presence of proteinaceous components from the papain. The peaks at 1450.47 cm^{-1} and 1411.89 cm^{-1} correspond to C–H bending and O–H deformation vibrations, respectively, which are characteristic of aliphatic and phenolic compounds from a*loe vera* phytoconstituents. The peaks at 1242.16 cm^{-1} and 1172.27 cm^{-1} are assigned to P=O and C–O–C stretching vibrations, respectively, indicative of phospholipid and carbohydrate interactions, respectively. A strong band at 1010.70 cm^{-1} further supports the presence of C–O stretching in the polysaccharides. Lower-frequency peaks between 794.67 cm^{-1} and 416.82 cm^{-1} are associated with aromatic and C–S vibrations, suggesting the presence of sulfur-containing amino acids in the papain.

The observed shifts and broadening of the amide and carbonyl peaks compared to those of the individual components imply hydrogen bonding and electrostatic interactions between papain, *aloe vera* constituents, and phospholipid molecules. These spectral shifts not only confirm the formation of intermolecular interactions but also reflect enhanced stability of the complex. Collectively, these findings confirmed the successful formation of the papain–*aloe vera* phytosomal complex in the formulation.

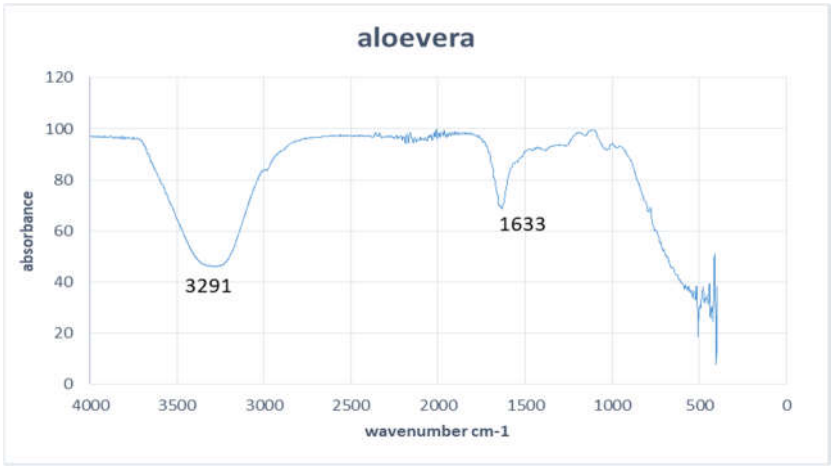

Fig. 1: The widest observed peak at wave numbers of 2900–3600 cm^{-1} is related to the stretching vibrations of the hydroxyl groups (O-H). The peak at 1633 cm^{-1} is attributed to the amide group. Multiple sharp and weak peaks observed below 500 cm^{-1} correspond to the skeletal vibrations of large biomolecules

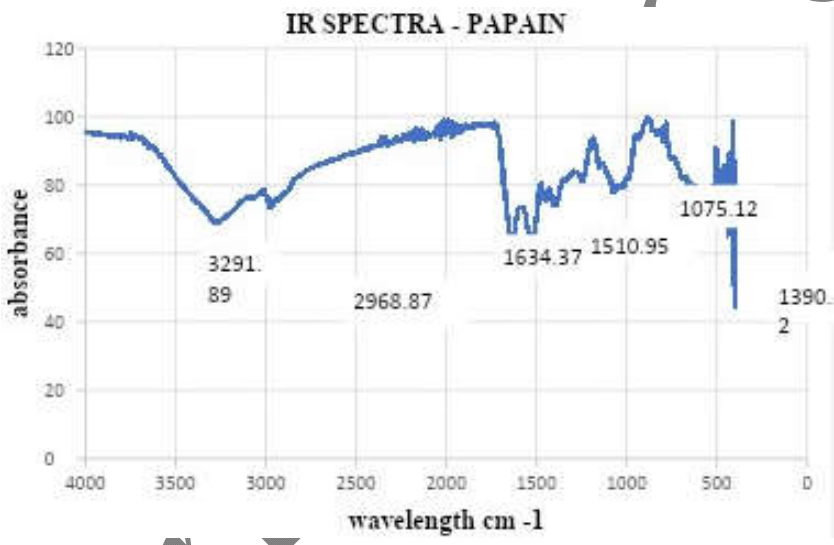

Fig. 2: FTIR spectrum showing peaks at 1634 cm^{-1} (amide C=O stretching), 1510 cm^{-1} (N–H bending and C–N stretching), and 1390 cm^{-1} (C–N stretching and N–H deformation), which are characteristic of amide groups

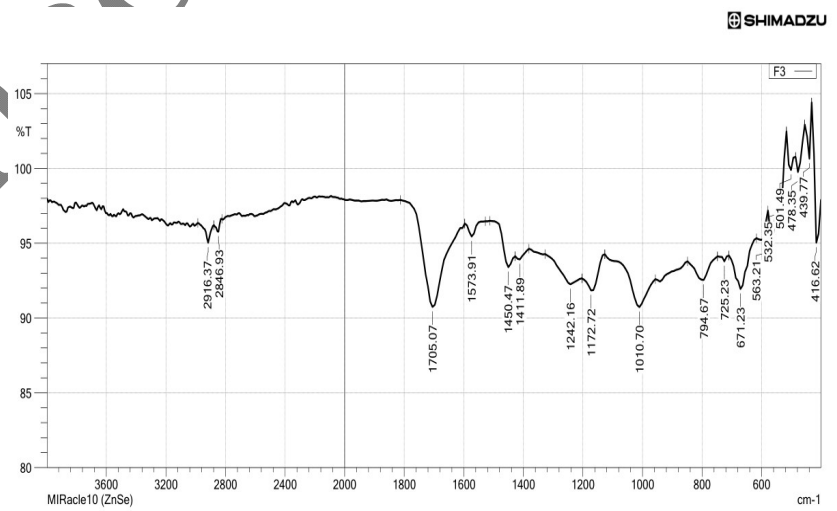

Fig. 3: (phytosome): 2916.37 cm^{-1} (asymmetric stretching vibrations of aliphatic C–H groups), 2848.93 cm^{-1} (symmetric stretching vibrations of aliphatic C–H groups), 1705.05 cm^{-1} (C=O stretching), 1242.16 cm^{-1} (O-C-O stretch), 1172.72 cm^{-1}(polysaccharide)

Table 2: Comparative FTIR peaks and functional group assignments of papain, *aloe vera* and papain–*aloe vera* phytosomal formulation

Component	Wavenumber (cm^{-1})	Functional group assignment	Remarks
Papain	568 and 432 cm^{-1}	C-S stretching	Presence of sulfur-containing amino acids
	1390 cm^{-1}	C–N stretching and N–H deformation	Presence of an amide group
	1510 cm^{-1}	N–H bending and C–N stretching	Presence of amide II
	1634 cm^{-1}	C=O stretching	Presence of amide I
	2968 cm^{-1}	Aliphatic C–H stretching	Presence of a methylene group
	3291 cm^{-1}	N–H stretching	Presence of amide II groups (protein backbone)
Aloe vera	1633 cm^{-1}	C=O stretching/H–O–H bending	Presence of amides/amino groups
extract	3291 cm^{-1}	O-H stretching	Presence of alcohol, phenol group
Phytosome	2916 cm^{-1}	Asymmetric C–H stretching	Long-chain hydrocarbon tails
	2848 cm^{-1}	Symmetric C–H stretching	Confirms lipid chains
	1705 cm^{-1}	C=O stretching	Carbonyl groups in amide
	1573.91 cm^{-1}	N–H bending and C–N stretching	Presence of papain (amide)
	1450 cm^{-1}	C–H bending	Aliphatic phytoconstituents
	1411 cm^{-1}	O–H deformation	Phenolic groups of aloe vera
	1242 cm^{-1}	P=O stretching	Phospholipid–biomole cule interaction
	1172 cm^{-1}	C–O–C stretching	Polysaccharide–phosp holipid interaction
	1010.70 cm^{-1}	C–O stretching	*Aloe vera* carbohydrate moieties
	794.67–416.82 cm^{-1}	C-S stretching	Sulfur-containing amino acids

The FTIR report indicates that the phytosomal formulation preserves all the significant peaks associated with papain and *aloe vera*. The minor shifts and broadening of the peaks observed can be attributed to the formation of papain–*aloe vera* phytosomes

Optimization of formulation variables

The independent variables were assigned levels of low (-1), medium (0), and high (+1) based on the outcomes of the preliminary trial. The experiments demonstrated that a combination of 25–75 mg of *aloe vera* extract and papain, along with 10–30 mg of phospholipid, effectively produced phytosomes with optimal particle size, a suitable PDI, and high entrapment efficiency.

Table 3: Experimental levels of independent variables (amount of *aloe vera* extract and papain, and the amount of phospholipid) in the design of experiments (DOE)

Independent variables	Low (mg)	Medium (mg)	High (mg)
Quantity of *aloe vera* extract	25	50	75
Quantity of papain	25	50	75
Phospholipid	10	20	30

Table 4: Experimental levels of responses [E E of *aloe vera* extract and papain, particle size (nm), and PDI] in the DOE

Responses	Low	High
EE of *aloe* extract *vera*	61.22	96.35
EE of papain	60.36	95.93
Particle size	87.3	830
PDI	0.225	0.653

E E-Entrapment efficiency PDI-Polydispersity index

A numerical optimisation study was performed using the desirability function approach to identify the most suitable combination of formulation variables for achieving maximum entrapment efficiencies, minimum particle size and PDI. Based on the composite desirability value, the optimised formulation consisted of 41.25 mg *aloe vera extract*, 46.25 mg papain, and 30 mg phospholipid, yielding a desirability score of

1.0. The model predicted a particle size of 62.24 nm, EE-P of 96.03%, EE-A of 96.47%, and a PDI of 0.146, indicating an optimal balance of all critical quality attributes. These results (table 5) suggest that the optimised formulation offers the most favourable physicochemical characteristics for further evaluation.

Table 5: Numerical optimisation of dual phytosome formulation showing the optimized actual factor levels and corresponding model-predicted responses obtained using desirability-based multi-response optimization

Parameter	Optimized actual value	Predicted response
Aloe vera extract (mg)	41.25 mg	
Papain (mg)	46.25 mg	
Phospholipid (mg)	30.00 mg	
Particle Size (nm)		62.24 nm
E E – papain (%)		96.03%
E E– a*loe vera* (%)		96.47%

PDI	0.146
Overall desirability	1.000 (Maximum)

E E-Entrapment efficiency PDI-Polydispersity index

Optimized solution (numerical results).

Coded factors: A = −0.35, B = −0.15, C =+1.00.

Actual factor levels:

Aloe vera extract = 50+25·A = 41.25 mg

Papain = 50+25·B = 46.25 mg

Phospholipid = 20+10·C = 30.00 mg

Polynomial response surface models in coded form (A, B, C = −1…+1) were used to perform multi-response numerical optimization. The models obtained from the box–behnken design are:

Polynomial equation — Particle size (nm)

Size= 160.40−43.73A−48.21B−25.71C+250.43AB−16.23AC+7.85BC+107.33A^2+105. 40B^2−128.15C^2

Polynomial equation — Entrapment efficiency of papain (EE-P%)

EE-P= 90.30+1.33A+4.48B+4.15C+1.28AB+7.08AC+0.38BC−17.24A^2−3.09B^2+7.36C^2

Polynomial equation — Entrapment efficiency of *aloe vera* (EE-A%)

EE-A= 91.60+2.90A+3.26B+3.29C+1.70AB+5.55AC−0.53BC−17.44A^2−4.16B^2+7.09C^2

Polynomial equation — PDI

PDI=0.312+0.0075A−0.0045B−0.0973C+0.054AB+0.0475AC−0.0335BC+0.1033A^2+0.1733B^2−0.0743C^2

These polynomial equations further helped in generating 2D and 3D response surface plots, which showed the same effects (fig. 4-11).

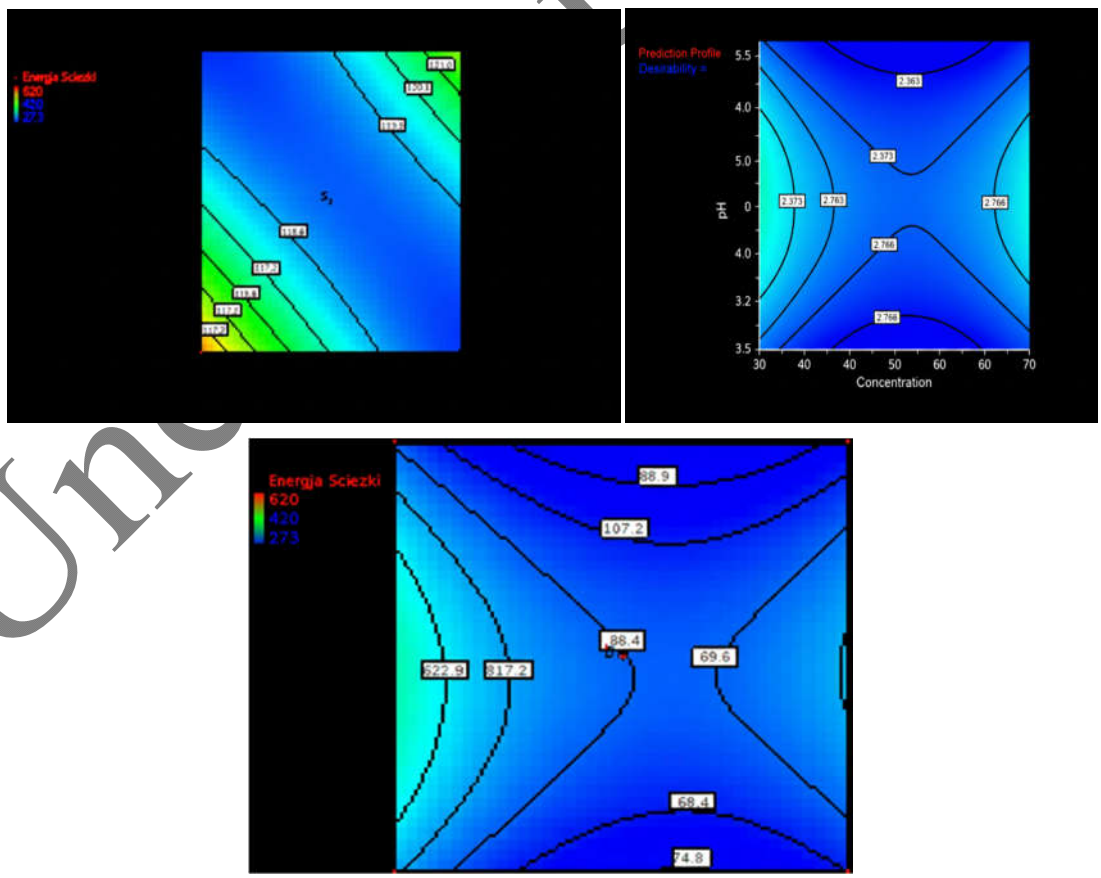

Fig. 4: Contour plots of particle size (2D). Contour plot showing the effect of formulation variables on particle size (nm). The color gradient represents variations in particle size, while contour lines indicate regions of equal particle size

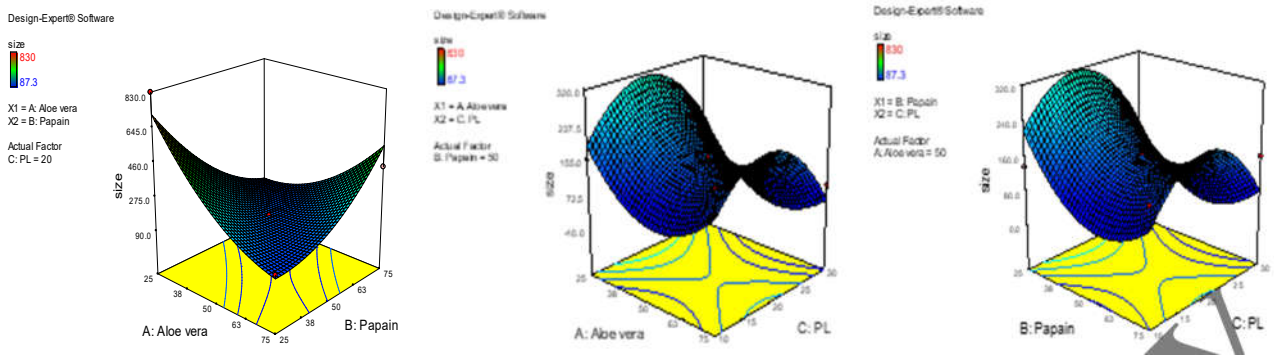

Fig. 5: 3D Response surface plots of particle size.3D. Response surface plot showing the effect of phospholipid concentration (A) and papain concentration (B) on vesicle size, an increase in phospholipid concentration resulted in a progressive increase in vesicle size, whereas higher papain levels tended to reduce particle size

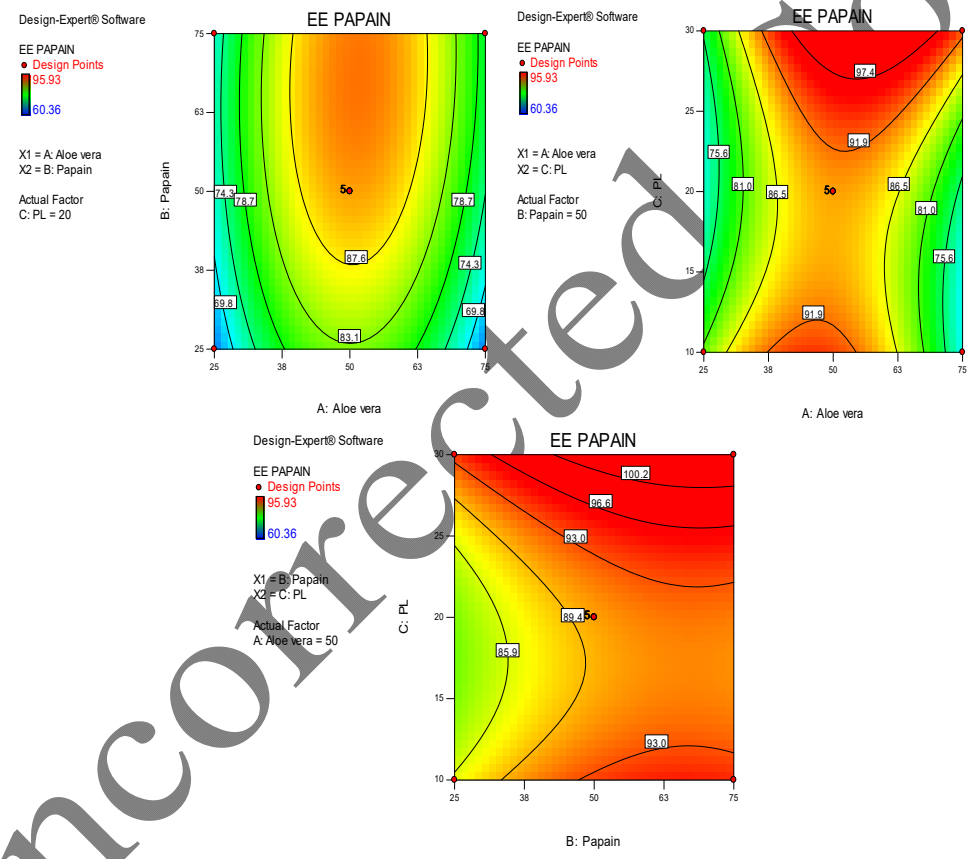

Fig. 6: Contour plot illustrating the effect of formulation variables on papain entrapment efficiency (2D)

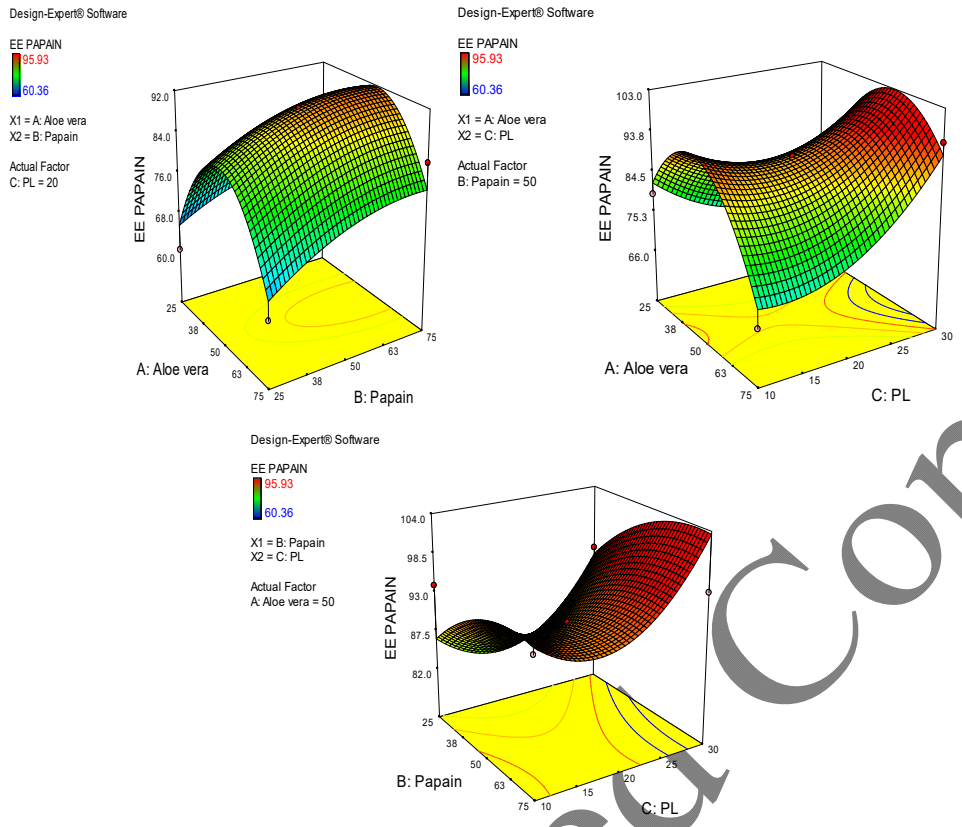

Fig. 7: 3D response surface plots of response surface plot illustrating the interaction between papain concentration (A) and phospholipid concentration (B) on papain entrapment efficiency. The curvature of the surface indicates a notable interaction between the two variables, emphasizing the importance of balanced composition for optimal drug loading

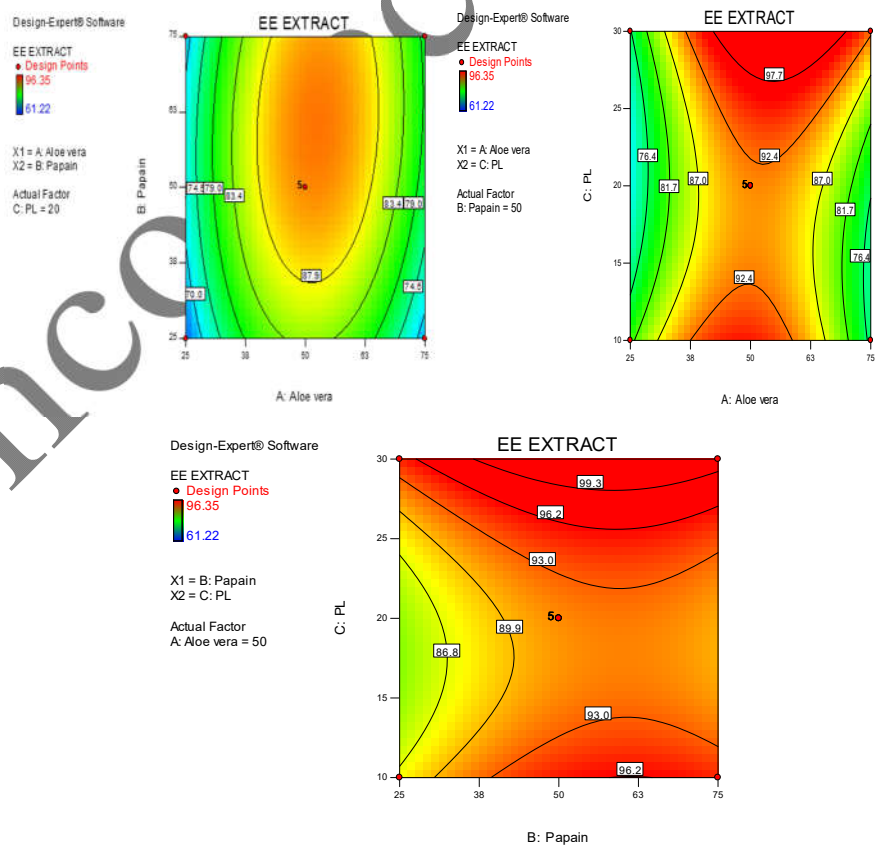

Fig. 8: Contour plot illustrating the effect of formulation variables on *aloe vera* entrapment efficiency (2D)

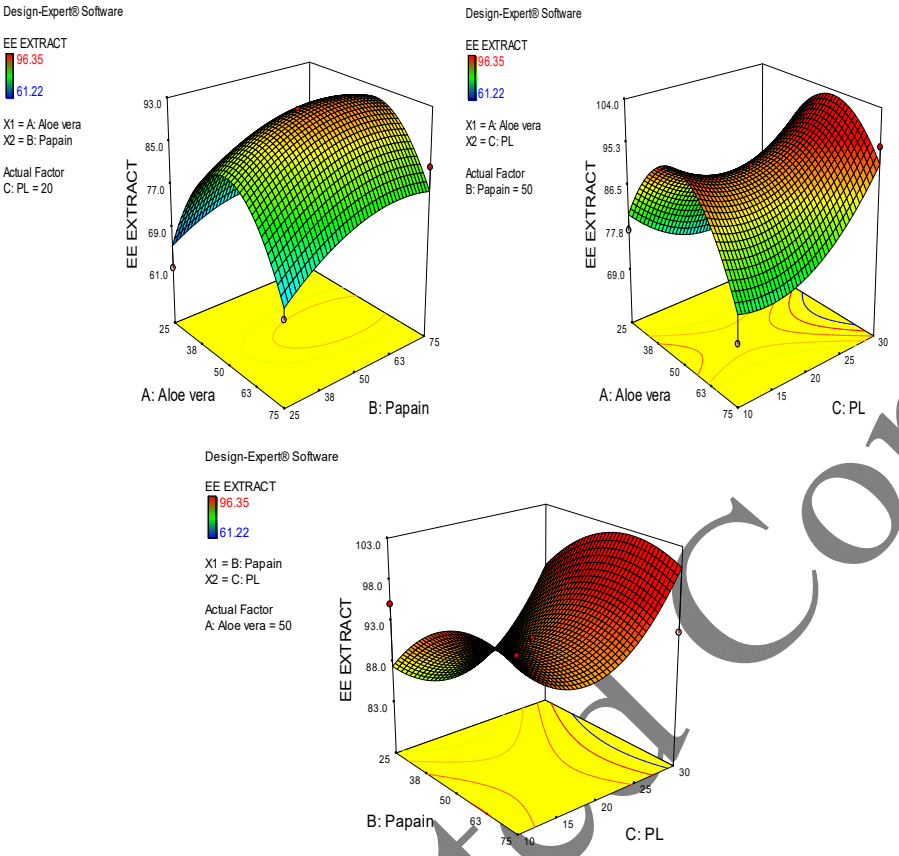

Fig. 9: 3D response surface plots of *aloe vera* entrapment efficiency

E E increased with increasing levels of both phospholipid and *aloe vera*. The ascending slope of the surface reflects a synergistic interaction between these factors, indicating their cooperative role in enhancing drug incorporation within the phytosomal vesicles.

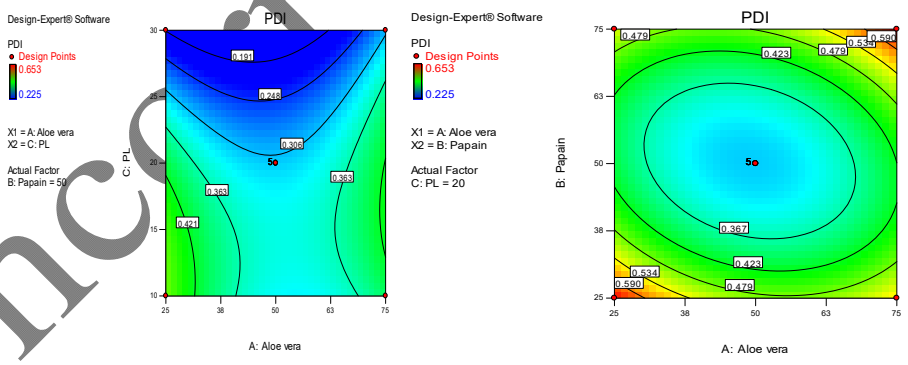

Fig. 10: Counter plots showing the effect of formulation variables on PDI (2D)

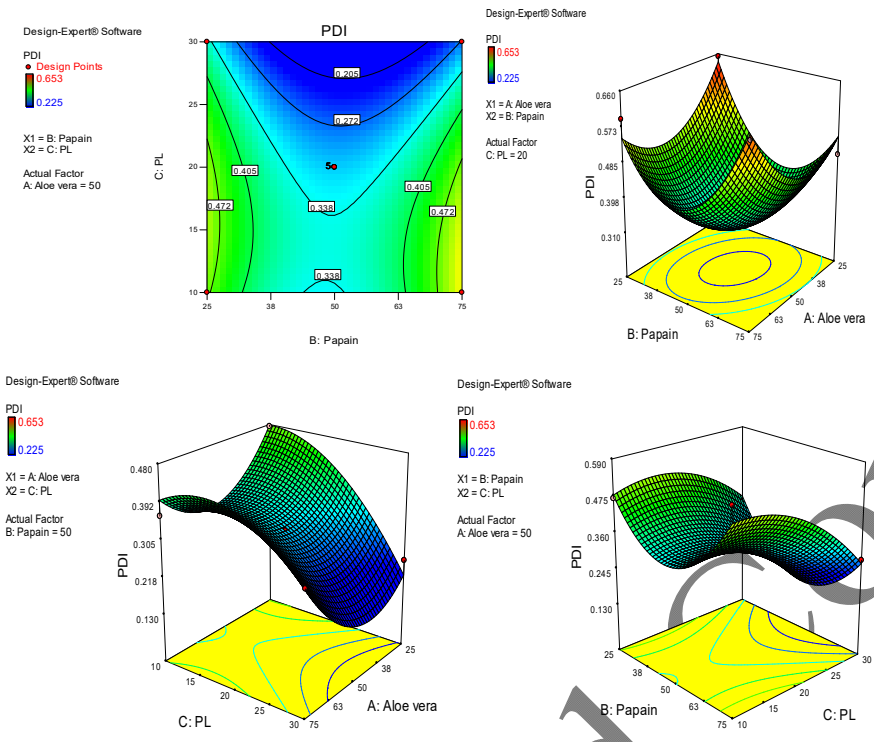

Fig. 11: 3D response surface plots of PDI

PDI decreased with increasing papain concentration, indicating improved vesicle uniformity. Conversely, higher *aloe vera* levels produced a slight increase in PDI. The elliptical contour pattern confirms a moderate interaction between the variables, demonstrating their combined influence on size homogeneity.

ANOVA-based model significance and adequacy

For each response, the computed model F-values were found to be high with $p<0.05$, indicating that the developed models were statistically significant and adequately described the relationship between the formulation factors and the measured responses. The non-significant lack-of-fit values further confirmed that the selected quadratic models were suitable for predicting responses within the studied range of variables. The coefficient of determination (R^2), adjusted R^2, and predicted R^2 values were all in close agreement, demonstrating the reliability and predictive ability of the models. The optimized region associated with F8 signifies the juncture at which variables such as *aloe vera* concentration, papain concentration, and phospholipid concentration attain an optimal synergistic ratio, thereby enhancing drug–lipid interaction and vesicle compactness. Collectively, the combined statistical validation, desirability-based optimization, and superior physicochemical performance unequivocally establish F8 as the optimal phytosomal formulation. Consequently, this formulation was selected for further development and subsequently incorporated into the gel system.

Preparation of *aloe vera*–papain phytosomes by the solvent evaporation method

Phytosomes are prepared by the solvent evaporation method as per table 6. Papain remains stable during solvent evaporation because it stays in the water-based part and is not soluble in dichloromethane (DCM). The lack of blending between the two phases limits direct contact between the solvent and the enzyme. Additionally, the surrounding matrix provides an extra layer of protection for papain.

Table 6: Detailed composition of the prepared phytosomal batches (F1–F17)

Code	*Aloe* vera extract mg	Papain mg	PC mg	Phosphate buffer ml	DCM ml
F1	25	25	20	4	6
F2	75	25	20	4	6
F3	25	75	20	4	6
F4	75	75	20	4	6
F5	25	50	10	4	6
F6	75	50	10	4	6
F7	25	50	30	4	6
F8	75	50	30	4	6
F9	50	25	10	4	6
F10	50	75	10	4	6
F11	50	25	30	4	6
F12	50	75	30	4	6
F13	50	50	20	4	6
F14	50	50	20	4	6
F15	50	50	20	4	6
F16	50	50	20	4	6

F17	50	50	20	4	6

PC – Phosphatidyl choline DCM-Dichloromethane

Particle size, polydispersity index, and entrapment efficiency

The optimized formulation was selected based on particle size, polydispersity index, and entrapment efficiency. The prepared phytosomes were spherical and discrete in shape.

The vesicles' particle size ranged from 87.3 nm to 1034 nm, with a PDI between 0.225 and 0.653, indicating a polydisperse system. The profound difference in the particle size of F1 and F8 is due to differences in papain concentration, *aloe vera* concentration, and phospholipid concentration. Here, F1 contain least amount of phospholipid, so complexation between drugs and phospholipid become week and poor encapsulation results. F8 formulation contains higher phospholipid content provided adequate bilayer stabilization, while the optimized loading of papain and *aloe vera* enhances hydrogen bonding and hydrophobic interactions within the phytosomal complex. The UV spectrophotometric methods used for the estimation of entrapment efficiency at 220 nm and 211 nm for papain and *aloe vera* extract were validated for linearity and repeatability. Both the analytes experience linear responses over the working concentration ranges, with correlation coefficients (R^2) more than 0.99 and adequate repeatability. The method exhibited acceptable sensitivity with limits of detection (LOD) and quantification (LOQ) determined as low nanogram levels. Accuracy was assessed by recovery studies at three concentration levels, yielding mean recoveries within 98–102%. The entrapment efficiency was between 60% and 96%. The results are presented in table 7, and the zeta potential report is shown in fig. 12.

Table 7: Particle size, entrapment efficiency, and PDI of different batches of phytosomes

Code	P. Size (nm)	E. E papain %	E. E *aloe vera* %	PDI
F1	1034±0.30	60.36±0.13	61.22±0.01	0.653±0.000
F2	146.1±0.35	62.03±0.02	65.86±0.01	0.593±0.001
F3	99.3±0.15	75.41±0.32	70.65±0.01	0.476±0.000
F4	265.4±0.30	82.08±0.01	82.21±0.20	0.632±0.001
F5	159.37±0.2	79.36±0.13	77.29±0.14	0.475±0.001
F6	200±0.26	66.39±0.31	69.70±0.44	0.362±0.001
F7	111.6±0.25	80.32±0.01	81.74±0.02	0.225±0.001
F8	87.3±0.05	95.62±0.01	96.35±0.01	0.302±0.001
F9	138.33±0.2	94.04±0.03	95.14±0.01	0.469±0.064
F10	159.6±0.29	93.57±0.02	96.31±0.00	0.587±0.001
F11	100±0.16	94.83±0.01	93.75±0.00	0302±0.001
F12	152.7±0.7	95.93±0.00	92.93±0.00	0.286±0.001
F13	160.4±0.12	90.30±0.17	91.57±0.01	0.312±0.001
F14	160.4±0.12	90.30±0.17	91.57±0.01	0.312±0.001
F15	160.4±0.12	90.30±0.17	91.57±0.01	0.312±0.001
F16	160.4±0.12	90.30±0.17	91.57±0.01	0.312±0.001
F17	160.4±0.12	90.30±0.17	91.57±0.01	0.312±0.001

Value are mean±SD, n=3, P. Size = Particle size, E E-Entrapment efficiency, PDI-Polydispersity index

A comparison between the predicted and experimentally observed (actual) values for the optimized formulation (F8)

The BBD's predicted values for particle size and entrapment efficiency were very close to the values found in experiments. The low % prediction error indicates that the polynomial model is good, reliable, and strong in predicting the responses. For nanovesicular systems, a variation of ≤30 to 40% in particle size is considered acceptable due to factors such as vesicle fusion, solvent evaporation kinetics, hydration dynamics, and variability in phospholipid–drug complexation. A deviation of ≤0.20 is taken as an acceptable value for the PDI. Entrapment efficiency result revealed that the model is very good at making predictions, with a deviation of ≤5%. PDI exhibited larger deviations from predicted values, with prediction errors of 106.85%. These higher errors suggest that the physical characteristics related to dispersion and size distribution may be more sensitive to subtle variations in formulation or processing conditions than predicted by the model. Overall, the model reliably predicts encapsulation efficiency outcomes and provides a strong basis for formulation optimization, while highlighting areas for empirical fine-tuning of size-related parameters. The values are given in table 8.

Table 8: Comparison of predicted and observed responses for optimized formulation (F8)

Response parameter	Predicted value	Observed value	%Prediction error
Particle size (nm)	62.24	87.3±0.05	40.28
E E– Papain (%)	96.03	96.35±0.01	0.33
E E– *Aloe vera* (%)	96.47	96.35±0.01	0.12
PDI	0.146	0.302±0.001	106.85

Value are mean±SD, n=3. E E-Entrapment efficiency, PDI-Polydispersity index

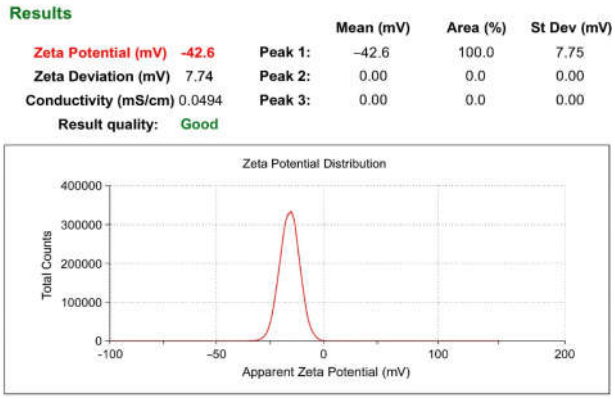

Fig. 12: Zeta potential distribution of the optimized dual-loaded papain *aloe vera* phytosomal formulation measured using a malvern zetasizer nano ZS90 (malvern instruments ltd., UK) value are mean±SD, n=3

Preparation of phytosomal gel

The composition of the optimized dual-loaded papain and *aloe vera* phytosomal gel is shown in table 9. Phytosomes containing both papain and *aloe vera* acted as the active ingredients, at a concentration of 1.5% w/w, ensuring optimal therapeutic effectiveness. Carbopol 940 (0.5% w/w) was used as the gelling agent. This provided the gel with the appropriate viscosity and consistency, facilitating easy application and prolonged adherence to the skin. Triethanolamine (1% w/w) was used as a stabilizer and neutralizer. This helped to adjust the pH of the formulation to approximately 6.4, which is within the physiological range, thus preventing irritation when applied to the skin. Propylene glycol (10% w/w) acted as a humectant, boosting skin hydration and improving the absorption of the active phytosomal complex. Methylparaben (0.09% w/w) was included as a preservative to prevent microbial growth and extend the shelf life of the formulation. The addition of vanilla essence (q. s.) provided a pleasant scent, increasing patient compliance and acceptance. Lastly, Aquadest (q. s.) was used as the solvent and dispersion medium, ensuring that all ingredients were evenly distributed throughout the gel.

Table 9: Composition of the dual-loaded papain–*aloe vera* phytosomal gel

Composition	Function	Quantity %
Phytosomes	Active ingredients	1.5
Carbopol 940	Gel base	0.5
Triethanolamine	Gel stabilizer	1
Propylene glycol	Humectant	10
Methyl paraben	Preservatives	0.09
Vanilla essence	Flavouring agent	qs
Aquadest	Solvent	qs

All ingredients were selected based on their compatibility with the dual phytosomal complex and their ability to enhance the physicochemical stability, spreadability, and user acceptability of the topical gel. The formulation aimed to achieve an optimal balance between viscosity, pH, and drug delivery efficiency for effective wound healing.

Particle size and PDI of phytosomal gel

Characterization of the phytosome formulation revealed an average particle size of 89.20 nm, indicating nanoscale dimensions suitable for enhanced bioavailability and targeted delivery. The PDI value of 0.445 suggests moderate polydispersity, indicating a relatively uniform particle size distribution. The presence of three distinct peaks in the size distribution indicates the coexistence of varying particle populations, with peak 1 (123.8 nm) dominating at 85.9%, followed by minor contributions from larger aggregates in peak 2 (4478 nm, 7.1%), and smaller particles in peak 3 (18.47 nm, 7.0%). The intercept value of 0.881 supports reliable measurements (fig. 13-14). These findings highlight the potential of the phytosome formulation for therapeutic applications, balancing nanoscale size with acceptable distribution uniformity. All the other results are given in table 10.

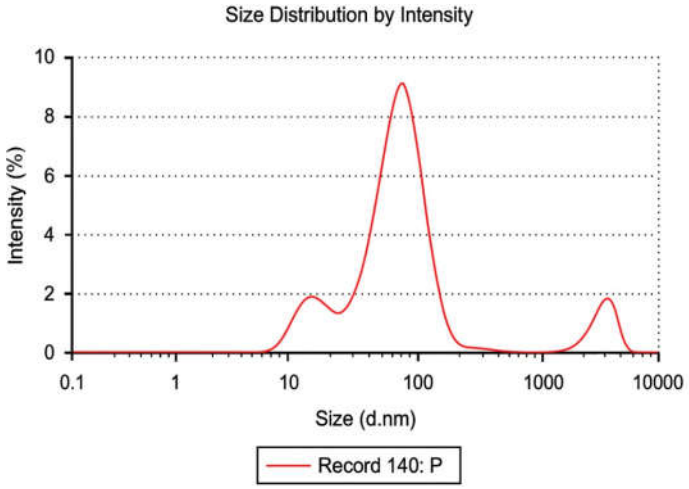

Fig. 13: Particle size distribution of phytosomal gel value are mean±SD, n=3

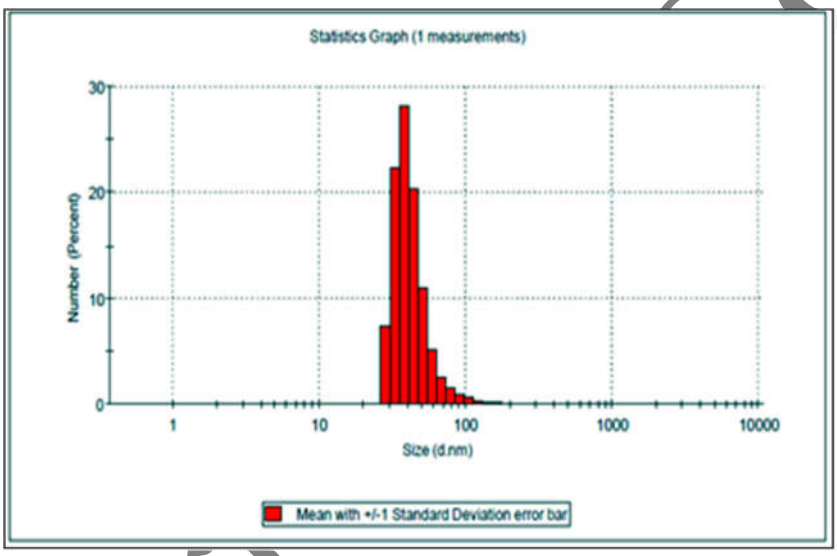

Fig. 14: Particle size distribution of phytosomal gel, values are mean±SD, n=3

Table 10: Evaluation parameters of phytosomal gel formulation

Parameter	Observation		Remarks
Organoleptic characteristics	Not sticky, Vanilla scent	Yellow,	Stable and aesthetically acceptable formulation.
pH	6.4±0.0577		Within physiological skin range; non-irritant.
Viscosity (Pa. s)	20.108±0.577		Suitable consistency for topical application.
Spreadability(g·cm/s)	21.08±0.5797		Good spreading property; easy to apply.
Entrapment efficiency (%)	86.3±0.3496		Efficient drug encapsulation within phytosomes.
Drug content (%)	89.23±0.4635		Acceptable range.
Particle size (nm)	89.20±0.4233		The nanometer range ensures better penetration and stability.
Polydispersity index (PDI)	0.445±0.000		Acceptable range
Pourability (%)	0.1±1.6996		Good flow property; easy to dispense.
Homogeneity	Homogeneous, coarse grained	no	Smooth and uniform texture.

Value are mean±SD, n=3, all parameters were evaluated for the optimized dual-loaded papain–*aloe vera* phytosomal gel. The results indicate that the formulation exhibits acceptable physicochemical characteristics, efficient drug encapsulation, uniform distribution, and overall suitability for topical application.

Zeta potential

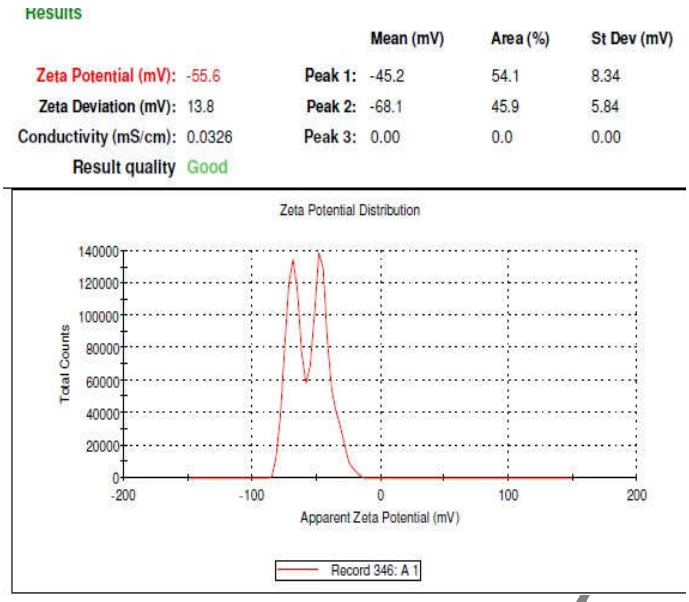

Fig. 15: Zeta potential distribution of *aloe vera*–papain dual-loaded phytosomal formulation, values are mean±SD, n=3

Scanning electron microscopy (SEM)

The SEM of the phytosomal gel is shown in fig. 16. The fig. indicates that particles are spherical with smooth surfaces. A smooth surface often indicates a well-formed lipid layer, while roughness could suggest incomplete encapsulation or instability of the formulation.

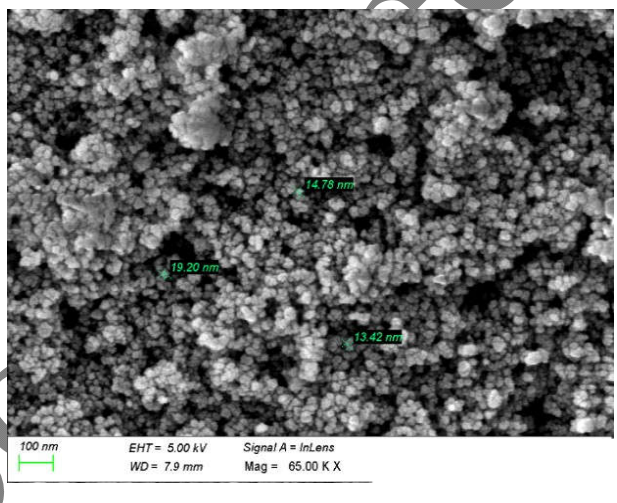

A

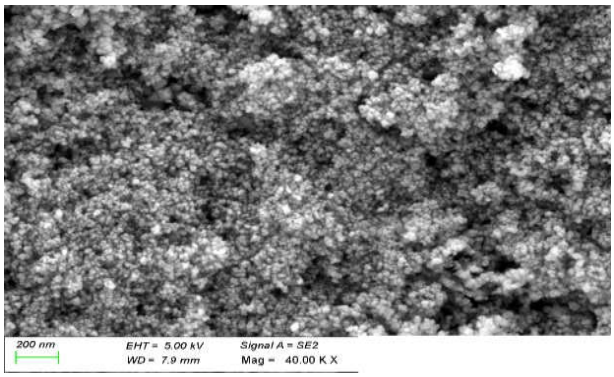

B

Fig. 16: SEM images of optimized phytosomal gel at different magnifications illustrating surface morphology and particle size distribution (A: 65,000×, scale bar: 100 nm; B: 40,000×, scale bar: 200 nm)

Differential scanning calorimeter (DSC) analysis

The DSC analysis of papain and *aloe vera* phytosomes reveals distinct thermal properties reflecting their structural characteristics. Papain exhibits an endothermic peak at 81.29 °C, with an onset at 76.84 °C and a normalized enthalpy of-87.42 J/g, indicating moderate thermal stability suitable for physiological applications but susceptible to denaturation at elevated temperatures. In contrast, the phytosomes show a high thermal stability with an endothermic peak at 289.25 °C, onset at 249.30 °C, and a significantly larger enthalpy change of-271.19 J/g, suggesting a robust molecular organization and efficient encapsulation of bioactive (fig. 17).

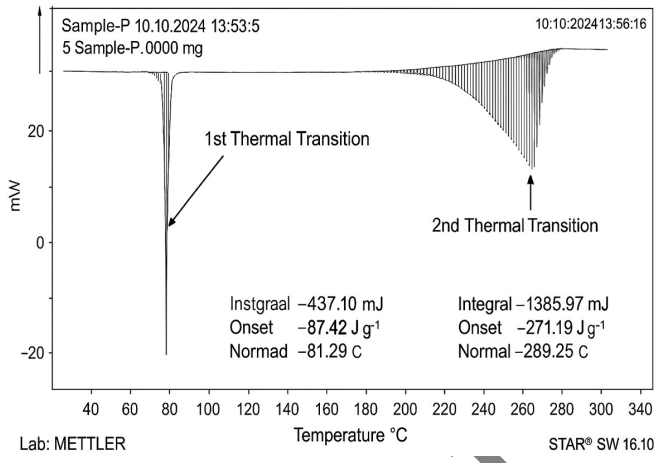

Fig. 17: DSC Image of formulation F8: showing an endothermic peak at 81.29 °C (onset at 76.84 °C) and a broad exothermic peak at 289.25 °C (onset at 249.30 °C), corresponding to enthalpy changes of-437.10 mJ and-1355.97 mJ, respectively

DPPH radical scavenging activity

The inhibition % of *aloe vera* extract (250 µg/ml) was 76.52% with an IC_{50} value of 105.32, papain (250 µg/ml) was 85.65% with an IC_{50} value of 65.70, ascorbic acid was 61.52% with an IC_{50} value of 189.10, and phytosome was 95.43% with an IC_{50} value of 35.33. The lower IC_{50} of the phytosome compared to *aloe vera* extract and papain alone confirms the enhanced antioxidant potential of the formulated system. This enhancement can be ascribed to the synergistic antioxidant properties of *aloe vera* phytoconstituents and papain, which collectively offer an expanded radical-scavenging capacity. Furthermore, phytosomal complexation with phospholipids enhances dispersion and lipid compatibility while protecting labile antioxidant groups from degradation, thereby increasing their effective availability during the DPPH assay. The DPPH radical scavenging activity (in percent) and IC_{50} values are shown in fig. 18-19.

What is number and weight distribution of particle size. What is number and weight distribution of particle size. What is number and weight distribution of particle size.

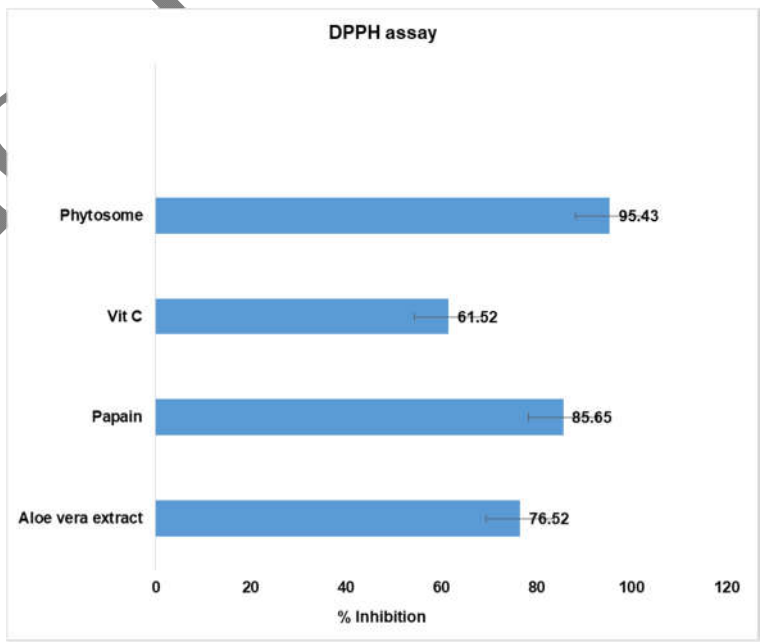

Fig. 18: DPPH radical scavenging activity of *aloe vera* extract, papain, phytosomal formulation, and ascorbic acid (standard), value **are expressed as mean±SD, n = 3. Statistical analysis was performed using two-way ANOVA followed by tukey's multiple comparison test (*p*<0.05)**

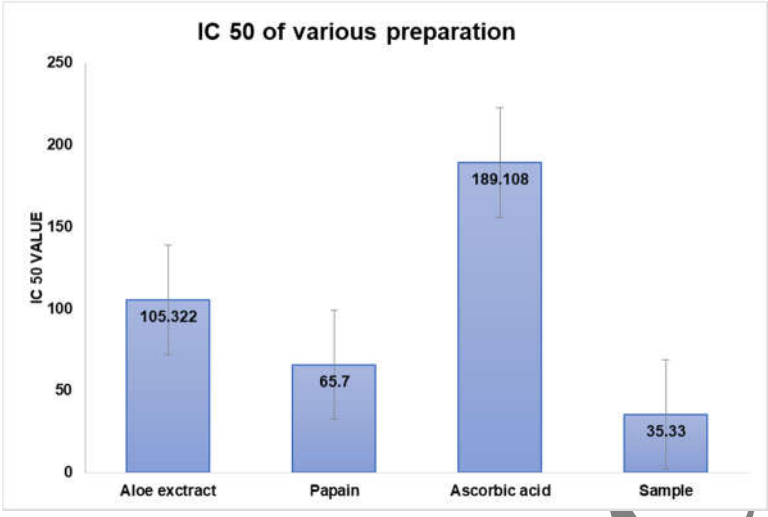

Fig. 19: IC_{50} values of *aloe vera* extract, papain, phytosome formulation, and ascorbic acid (control) from the DPPH assay. value **are expressed as mean±SD, n = 3. Statistical analysis was performed using one-way ANOVA followed by tukey's multiple comparison test (*p*<0.05)**

The phytosome showed the highest antioxidant activity with the lowest IC_{50}.

α-amylase inhibition

The phytosome demonstrated a concentration-dependent α-amylase inhibition (0-125 µg/ml). This gradual increase in inhibition highlights the dose-responsive activity of the preparation, achieving up to 56% inhibition at 125 µg/ml, which is significantly higher than the negative control but slightly lower than the positive control (66%) at the same concentration. Acarbose, a well-known α-amylase inhibitor, served as a benchmark and demonstrated superior inhibitory effects across all tested concentrations. The result is summarised in table 11-13.

Table 11: α-amylase Inhibition of control

Concentration (µg/ml)	%Inhibition
0	0±0.0
25	2±0.2
50	4±0.5
75	5.4±0.1
100	6.7±1.9
125	6.9±1.2

Value are expressed as mean±SD, n = 3.

Table 12: α-amylase Inhibition of phytosome

Concentration (µg/ml)	% Inhibition
0	0±0
25	29±2.22
50	33±4.19
75	42±3.9
100	53±7.9
125	56±9.19

Value are expressed as mean±SD, n = 3.

Table 13: α-amylase Inhibition of acarbose (positive control)

Concentration (µg/ml)	% Inhibition
0	0±3.0
25	27±5.9
50	46±6.19
75	54±7.1
100	57±8.19

125	66±9.2

Value are expressed as mean±SD, n = 3. Statistical analysis was performed using two-way ANOVA followed by tukey's multiple comparison test (p<0.05)

Statistical analysis

Treatment type, concentration, and interaction significantly influence α-amylase inhibition (p<0.0001). The control exhibited minimal activity, confirming assay specificity. The result is summarised in table 14.

Table 14: Statistical assay α-amylase inhibition

Source of variation	DF	F-valu e	P-value	Significance
Treatment (between groups)	2	189.2	<0.0001	****
Concentrat ion (within groups)	5	204.8	<0.0001	****
Interaction (Tx × Conc.)	10	11.4	<0.0001	****
Residual (Error)	36	—	—	—

**** indicates highly significant differences at p<0.0001.

Cell viability measurement (MTT ASSAY)

OD readings were obtained at 570 nm for a range of concentrations (6.25 to 100 µg/ml). Percentage cell viability was calculated relative to untreated control cells, which exhibited an average OD of 0.70, corresponding to 100% viability. A dose-dependent decrease in viability was observed with increasing concentrations of the phytosome, with the lowest viability (~85.71%) recorded at 100 µg/ml (average OD = 0.6). Povidone-iodine was selected as the positive control because it is routinely applied in clinical wound management, making it a clinically relevant comparator for assessing fibroblast viability and biocompatibility of wound-care formulations. Statistical analysis showed no significant difference in cell viability between the two treatments (p>0.05) at concentrations above 6.25 µg/ml, underscoring the formulation's biocompatibility. The triplicate measurements exhibited low standard deviations and standard errors, confirming the reproducibility and reliability of the data. The results are summarized in table 15.

Table 15: MTT assay-impact of sample concentration on cell viability

Sample µg/ml	OD	% viability
6.25	0.67	96.2
12.5	0.66	94.28
25	0.65	93.8
50	0.64	91.42
100	0.6	85.71
Standard-povidone iodine		
6.25	0.62	89.52
12.5	0.59	84.76
25	0.58	82.85
50	0.57	82.38
100	0.56	80.00

Both test and standard maintained>80% viability in a concentration-dependent manner. Blank (untreated cells) showed 100% viability. Data are expressed as mean±SD, n = 3. Statistical analysis was performed using one-way ANOVA followed by tukey's multiple comparison test (p<0.05).

Statistical analysis

One-way ANOVA revealed a statistically significant difference between the treatment concentrations (p<0.0001). Tukey's post-hoc test indicated that at 100 µg/ml, cell viability was significantly lower compared to the control (*p<0.01*), though comparable to the standard Povidone-Iodine." The result is shown in table 16.

Table 16: Statistical analysis (ANOVA summary)

Source of variation	Sum of square s (SS)	Deg rees of free do m (DF)	Mean squ are (MS)	Fval ue	P-value
Between groups	820.85	4	205.21	86.22	<0.0001
Within groups	23.75	10	2.38		
Total	844.6	14			

One-way ANOVA showed a highly significant difference among groups (P<0.0001)

Stability studies

The phytosomes showed no significant signs of drug degradation, demonstrating stability over six months. During this time, their physical appearance, particle size, and entrapment efficiency remained relatively unchanged. The PDI value of the gel formulation increased from 0.303 to

0.365, and from 0.303 to 0.412 at 40 °C±2 °C/75 % RH±5 % RH. For a nanoscale topical application, a PDI value of up to 0.5 is usually fine. Unlike intravenous systems, where a high PDI can raise safety concerns due to systemic circulation, topical formulations applied directly to the skin are far less sensitive to moderate size variation. The formulation maintained stability for six months when stored in a sealed amber bottle. Table 17 presents the findings.

Table 17: Stability profile of phytosomal gel at different storage temperatures

Time (M)	Temperature (°C)	P. size (nm)	EE (%)	PDI
0	30 °C±2 °C/65% RH±5% RH	87.26±0.002	96.0±0.054	0.303±0.032
0	40 °C±2 °C/75% RH±5% RH	87.26±0.002	96.0±0.054	0.303±0.032
1	30 °C±2 °C/65% RH±5% RH	89.1±0.017	95.24±0.05	0.309±0.032
1	40 °C±2 °C/75% RH±5% RH	94.2±0.047	94.19±0.07	0.312±0.032
3	30 °C±2 °C/65% RH±5% RH	91.5±0.023	93.49±0.024	0.319±0.034
3	40 °C±2 °C/75% RH±5% RH	96.7±0.023	93.25±0.004	0.327±0.035
6	30 °C±2 °C/65% RH±5% RH	101.43±0.013	89.78±0.069	0.365±0.033
6	40 °C±2 °C/75% RH±5% RH	111.73±0.012	87.98±0.040	0.412±0.000

Value are mean± SD, n=3, P. Size – Particle size, RH – Relative humidity, Time in month.

Diabetic wound healing activity

The wound healing activity of the test samples was evaluated using an excision wound model in wistar rats.

Table 18: *In vivo* study design

S. No.	Groups	Number of animals
I	Diabetic control	6
II	Standard	6
III	Test sample low dose	6
IV	Test sample high Dose	6
Total number of animals		24

Standard-Purilon® gel (coloplast)

Effect on body weight

The body weights of the animals were monitored on 0, 1, 7, 14, 21, and 28 d (d), as shown in table 19. No significant differences in body weight were observed among the animals throughout the study. All animals demonstrated a normal increase in body weight.

Table 19: Effect of test samples on body weight

Groups	D0	D 1	D 7	D 14	D 21	D 28
Group I-Contro l	191.33±2.66	191.5±3.15	195.33±2.73	203.33±4.08	204.33±3.08	206.67±2.94
Group II-Standard	191.5±2.95	191.67±3.01	193.83±2.48	197.5±2.66	201.5±2.51	207.60±2.14
Group III-Test low dose	192.5±7.4	192.67±6.89	196.17±3.66	201±2.37	205.83±1.47	209.67±1.97
Group IV-Test high dose	193.33±1.75	194.17±1.83	196.67±1.86	200.17±1.83	203±1.79	207.00±2.19

Value are Mean± SD, n=6. Statistical analysis was performed using two-way ANOVA followed by tukey's multiple comparison test. *p<0.05, statistically significant compared with standard (Purilon® gel)

Effect on wound area

The wound area was measured on day 0,1, 5, 9, 13, 17, 21, and 25, as shown in table 20. No significant difference in the wound area was observed on days 0 and 1. However, a significant decrease in wound area was observed from day 5 to day 25 in all the treatment groups compared to group I. Group IV showed a more significant difference in wound area compared to group I. The percentage of wound closure was calculated from the wound area on day 0,1,5,9,13,17, 21, and 25, as shown in table 21 and fig. 20. Epithelialization was observed on days 18, 23, and 19 for groups II, III, and IV, respectively.

Table 20: Effect of test samples on wound area

Day	Group I control	Group II standard	Group III test low dose	Group IV test high dose
D 0	501.17±0.98	501.5±1.52	502.17±1.47	501.33±1.21
D 1	495.17±2.48	493.83±2.48	492.67±2.8	494±3.03
D 5	457±7.4	435.5±3.73*	448.5±15.06	419.83±9.26*
D 9	419.17±13.56	342.83±14.54*	394±11.3*	262.83±11.87*
D 13	348.5±21.07	254.17±6.43*	279.83±13.35*	174.67±13.97*
D 17	272.5±8.96	136.17±7.17*	179.5±12.6*	39.67±8.85*
D 21	146.33±14.01	30.83±2.79*	54±8.29*	0.5±0.84*

D 25	92.5±10.62	0.33±0.52*	0.6±0.89*	0±0*
Epithelialization	29.17±0.75	18.67±1.63*	23.17±0.98*	19.33±1.37*

Value are Mean± SD, n=6; * Group I Vs Group II, III and IV; p<0.05, two-way ANOVA followed by tukey's multiple comparison test.

Table 21: Effect of test samples on percentage wound closure

Day	Group I control	Group II STD	Group III low test dose	Group III Test high hose
Day 0	0±0	0±0	0±0	0±0
Day 1	1.2±0.5	1.53±0.5	1.89±0.61	1.46±0.75
Day 5	8.81±1.62	13.16±0.84	10.69±2.99	16.26±1.81*
Day 9	16.36±2.88	31.64±2.95	21.54±2.29*	47.58±2.31*
Day 13	30.46±4.29	49.32±1.4	44.27±2.72*	65.16±2.74*
Day 17	45.63±1.82	72.85±1.47	64.25±2.54*	92.09±1.77*
Day 21	70.8±2.78	93.85±0.56	89.25±1.64*	99.9±0.17*
Day 25	81.54±2.14	99.93±0.1	99.9±0.17*	100±0*

Value are mean±SD, n=6; * group I Vs group II, III, and IV; p<0.05, two-way ANOVA followed by tukey's multiple comparison test

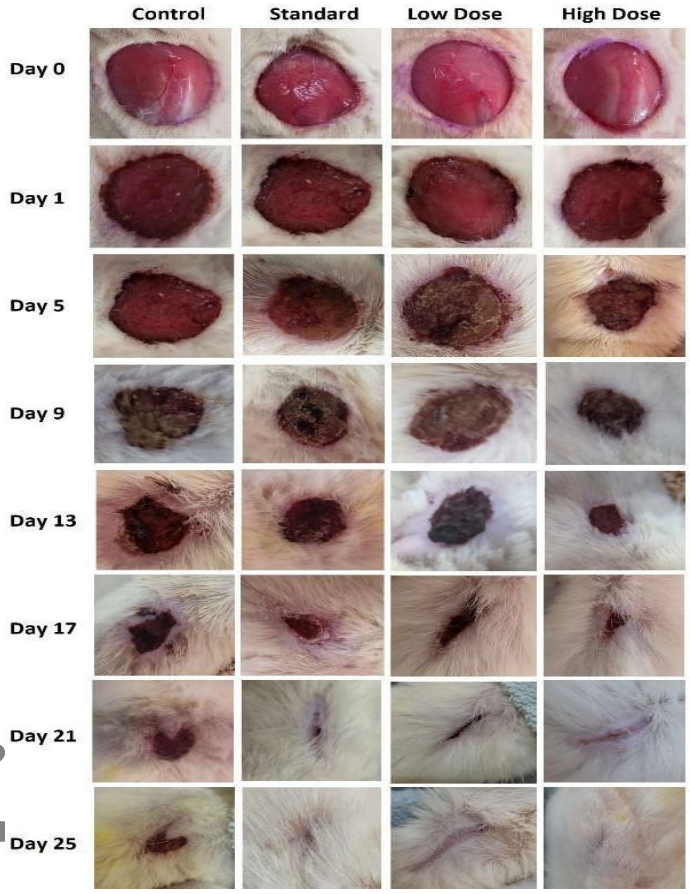

Fig. 20: Effect of test samples on wound contraction

Representative photographic images showing the time-dependent healing pattern of excisional wounds in the control, standard (Coloplast purilon gel), low-dose, and high-dose treated groups at predetermined intervals (Day 0, 1, 5, 9, 13, 17, 21, and 25 post-wounding). The control group showed the lowest percentage of wound contraction throughout the study period, with incomplete closure even on Day 25. Treatment with the purilon gel resulted in a moderate but significant improvement in wound contraction compared to control (p<0.05). In contrast, the low-dose formulation produced a significantly higher percentage of wound contraction from Day 9 onward, while the high-dose group exhibited the greatest contraction, achieving near-complete wound closure by Day 21. These findings are in agreement with previous reports demonstrating enhanced wound repair following nano-enabled phytotherapeutic interventions that promote fibroblast activity, collagen deposition, and re-epithelialization.

Histopathology

The histopathological features of the skin tissue of all groups were examined under a motic microscope (20x). Group I (control) animals showed inflammatory cells, reduced collagen fibers, fibroblast cells, blood vessels, and visible scar tissue (fig. 20). Groups II (standard) and group IV (Test-high dose) showed increased fibroblast cell regeneration, collagen fibers, and blood vessels. Group IV demonstrated more significant wound healing than the control group (group I) and other treatments. Coloplast purilon® gel is used as a standard.

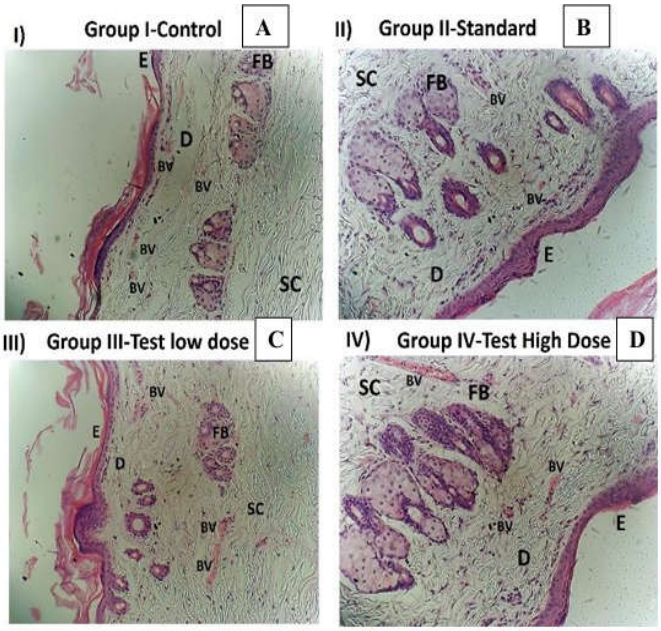

Fig. 21: Histopathological evaluation of skin tissue A) Group I-Control, B) Group II-Standard (Purilon gel), C) Group III-Test low dose, D) Group IV-Test high dose; E-Epidermis, D-Dermis, SC-Subcutaneous, BV-Blood vessels (Angiogenesis), FB-Fibroblast cell

The findings of the present study are consistent with earlier reports demonstrating the therapeutic potential of plant-derived bioactive compounds in diabetic wound healing. Daburkar *et al.* [21] reported that administration of *aloe vera* gel ethanolic extract in streptozotocin-induced diabetic rats significantly enhanced wound healing by promoting fibroplasia, collagen synthesis, and wound contraction. The authors also observed a significant reduction in fasting blood glucose levels and an improvement in plasma insulin following oral administration of the extract, suggesting that the hypoglycemic effect of *aloe vera* may indirectly contribute to improved wound repair in diabetes. Similarly, Li *et al.* [22] demonstrated that extracts from different parts of *carica papaya* possess both anti-diabetic and wound-healing properties. Their *in vitro* study revealed enhanced glucose uptake in liver and myoblast cells along with increased fibroblast migration and collagen production, indicating a stimulatory effect on cellular processes involved in tissue regeneration. In agreement with these findings, the results of the present study also indicate enhanced wound-healing activity, which may be attributed to stimulation of fibroblast proliferation, increased collagen deposition, and improved wound contraction. The observed therapeutic effect may therefore be associated with the presence of bioactive phytochemicals that facilitate tissue regeneration and modulate metabolic disturbances associated with diabetes, thereby accelerating the wound-healing process. Importantly, the present study demonstrates that formulation of papain and *aloe vera* into a phytosomal gel system can significantly improve the therapeutic potential of these phytoconstituents by enhancing skin permeation and enabling sustained release at the wound site. Therefore, the developed papain–*aloe vera* phytosomal gel may serve as a promising topical delivery system for enhancing the therapeutic efficacy of plant-derived bioactives in diabetic wound management.

CONCLUSION

This study successfully developed and optimized a dual-loaded *aloe vera*–papain phytosomal formulation using the solvent evaporation method and a Box–behnken design. The optimized phytosomes exhibited favourable physicochemical characteristics, including nano-sized particles, high entrapment efficiency, and good colloidal stability, with FTIR and DSC confirming stable complex formation. The prepared phytosomal gel showed measurable *in vitro* antioxidant and amylase inhibitory activity. But its amylase inhibitory action was not very good compared to standard insulin, as expected for a non-systemic topical preparation

Phytosomal gel-treated groups showed considerably faster wound healing in comparison to control and standard therapy in the streptozotocin-induced diabetic rat model. The therapeutic efficacy was further substantiated by increased collagen deposition, fibroblast proliferation, and angiogenesis. Overall, the optimized phytosomal gel showed superior wound-healing performance in a diabetic rat model, supporting its potential as a safe and effective topical formulation for diabetic wound management. A limitation of the study is the absence of detailed mechanistic pathway investigations and the use of a single animal model.

FUTURE RESEARCH DIRECTIONS

Future research should aim to address these gaps by incorporating multiple animal models that are relevant to different clinical disorders. Exploring the underlying mechanisms in greater depth could lead to a more comprehensive understanding of the phenomena observed and enhance the applicability of the findings. To facilitate clinical application and large-scale manufacturing, a comprehensive investigation into the cutaneous absorption, systemic activity, and long-term stability of the pharmaceutical agent is essential. Clinical trials are to be conducted to show that this treatment works better than alternative ways to care for wounds.

ACKNOWLEDGMENT

During the preparation of this work, the author(s) used open AI tools like chatGPT for language editing and fig. improvement. All AI-generated content was carefully reviewed, edited, and validated by the authors, who take full responsibility for the accuracy, originality, and integrity of the final manuscript.

FUNDING

No funding was received at any stage of this work.

ETHICS STATEMENT

The study protocol was reviewed and approved by the institutional animal ethics committee (IAEC) of JSS college of pharmacy, ooty-643001, tamil Nadu, india, under approval number JSSCP/OT/IAEC/13/2025-26. Every effort was made to minimize animal suffering and reduce the number of animals used.

AUTHORS CONTRIBUTIONS

Saurabh Singh: conceptualization, methodology, supervision. Sajisha VS: conceptualization, conduct of experiment, original draft Preparation. Aswin EV: Data curation, critical proofreading, review, and significant modifications in the final draft. Sheetu Wadhwa: Critical proofreading and modification in the final draft.

CONFLICT OF INTERESTS

The authors declare no conflict of interest

REFERENCES

1. Oguntibeju OO. Medicinal plants and their effects on diabetic wound healing. Vet World. 2019;12(5):653-63. doi: 10.14202/vetworld.2019.653-663, PMID 31327900.
2. Safta DA, Bogdan C, Moldovan ML. Vesicular nanocarriers for phytocompounds in wound care: preparation and characterization. Pharmaceutics. 2022;14(5):991. doi: 10.3390/pharmaceutics14050991, PMID 35631577.
3. Nandhini S, Ilango K. Development and characterization of a nano-drug delivery system containing vasaka phospholipid complex to improve bioavailability using quality by design approach. Res Pharm Sci. 2021;16(1):103-17. doi: 10.4103/1735-5362.305193, PMID 33953779.
4. Ezhilarasu H, Vishalli D, Dheen ST, Bay BH, Srinivasan DK. Nanoparticle-based therapeutic approach for diabetic wound healing. Nanomaterials (Basel). 2020 Jun;10(6):1234. doi: 10.3390/nano10061234, PMID 32630377 In: https://www. mdpi. com/2079-4991/10/6/1234.
5. Islam N, Irfan M, Hussain T, Mushtaq M, Khan IU, Yousaf AM et al. Piperine phytosomes for bioavailability enhancement of domperidone. J Liposome Res. 2022;32(2):172-80. doi: 10.1080/08982104.2021.1918153, PMID 33944662.
6. Huang Z, Brennan CS, Zhao H, Liu J, Guan W, Mohan MS et al. Fabrication and assessment of milk phospholipid-complexed antioxidant phytosomes with vitamin C and E: A comparison with liposomes. Food Chem. 2020;324:126837. doi: 10.1016/j.foodchem.2020.126837.
7. Shriram RG, Moin A, Alotaibi HF, Khafagy ES, Al Saqr A, Abu Lila AS et al. Phytosomes as a plausible nano-delivery system for enhanced oral bioavailability and improved hepatoprotective activity of silymarin. Pharmaceuticals (Basel). 2022;15(7):790. doi: 10.3390/ph15070790, PMID 35890088.
8. Haghani F, Arabnezhad MR, Mohammadi S, Ghaffarian-Bahraman A. *Aloe vera* and streptozotocin-induced diabetes mellitus. Rev Bras Farmacogn. 2022;32(2):174-87. doi: 10.1007/s43450-022-00231-3, PMID 35287334.
9. Roney M, Issahaku AR, Govinden U, Gazali AM, Aluwi MF, Zamri NB. Diabetic wound healing of aloe vera major phytoconstituents through TGF-β1 suppression via in-silico docking, molecular dynamic simulation and pharmacokinetic studies. J Biomol Struct Dyn [Internet]. 2024 Dec 20;42(24):13939-52. doi: 10.1080/07391102.2023.2279280, PMID 37942697 In: https://www. tandfonline. com/doi/full/10.1080/07391102.2023.2279280.
10. Wahedi HM, Jeong M, Chae JK, Do SG, Yoon H, Kim SY. Aloesin from *Aloe vera* accelerates skin wound healing by modulating MAPK/Rho and Smad signaling pathways *in vitro* and *in vivo*. Phytomedicine. 2017;28:19-26. doi: 10.1016/j.phymed.2017.02.005, PMID 28478809.
11. Muñiz-Ramirez A, Perez RM, Garcia E, Garcia FE. Antidiabetic activity of *Aloe vera* Leaves. Evid Based Complement Alternat Med. 2020 Jan;2020:6371201. doi: 10.1155/2020/6371201, PMID 32565868.
12. Melenshia DS, Amirtham SM, Rebekah G, Vinod E, Kachroo U. Effect of reconstituted, lyophilized cold aqueous extract of Aloe vera on human whole blood clotting time – A pilot study. J Ayurveda Integr Med. 2024;15(2):100887. doi: 10.1016/j.jaim.2024.100887, PMID 38479038.
13. Daburkar M, Lohar V, Rathore AS, Bhutada P, Tangadpaliwar S. An *in vivo* and *in vitro* investigation of the effect of *Aloe vera* gel ethanolic extract using animal model with diabetic foot ulcer. J Pharm Bioallied Sci. 2014;6(3):205-12. doi: 10.4103/0975-7406.135248, PMID 25035641.
14. Govindarajan S, Babu SN, Vijayalakshmi MA, Manohar P, Noor A. *Aloe vera* carbohydrates regulate glucose metabolism through improved glycogen synthesis and downregulation of hepatic gluconeogenesis in diabetic rats. J Ethnopharmacol. 2021;281:114556. doi: 10.1016/j.jep.2021.114556, PMID 34438036 In: https://www. Com/science/article/abs/pii/S0378874121007856. ScienceDirect.
15. Haasbroek A, Willers C, Glyn M, Du Plessis L, Hamman J. Intestinal drug absorption enhancement by *Aloe vera* gel and whole leaf extract: *in vitro* investigations into the mechanisms of action. Pharmaceutics. 2019;11(1):36. doi: 10.3390/pharmaceutics11010036, PMID 30669246.
16. Le Phan TH, Park SY, Jung HJ, Kim MW, Cho E, Shim KS et al. The role of processed *Aloe vera* gel in intestinal tight junction: an *in vivo* and *in vitro* study. Int J Mol Sci. 2021;22(12):6515. doi: 10.3390/ijms22126515, PMID 34204534.
17. Nayak BS, Ramdeen R, Adogwa A, Ramsubhag A, Marshall JR. Wound-healing potential of an ethanol extract of *Carica papaya* (Caricaceae) seeds. Int Wound J. 2012 Dec;9(6):650-5. doi: 10.1111/j.1742-481X.2011.00933.x. PMID 22296524.
18. Hersi F, Sebastian A, Tarazi H, Srinivasulu V, Mostafa A, Allayeh AK et al. Discovery of novel papain-like protease inhibitors for potential treatment of COVID-19. Eur J Med Chem. 2023;254:115380. doi: 10.1016/j.ejmech.2023.115380, PMID 37075625 In: https://www. Com/science/article/pii/S022352342300346X. ScienceDirect.
19. Chandan C, Phani Kumar G, Jawahar N, Sushma BV, Amachawadi RG, Shati AA et al. Design, development and characterization of papain-loaded nanostructured lipid carriers for enhanced stability and bio-accessibility in acidic environments. Results Chem. 2024;8:101571. doi: 10.1016/j.rechem.2024.101571.
20. Langer V, Bhandari PS, Rajagopalan S, Mukherjee MK. Enzymatic debridement of large burn wounds with papain-urea: is it safe? Med J Armed Forces India. 2013;69(2):144-50. doi: 10.1016/j.mjafi.2012.09.001, PMID 24600088.
21. Li H, Beg OU, Rafie AR, Kanwal S, Ovalle-Cisneros A, Faison MO et al. Characterization of green and yellow papaya (*Carica papaya*) for anti-diabetic activity in liver and myoblast cells and wound-healing activity in fibroblast cells. Nutrients. 2023 Apr 17;15(8):1929. doi: 10.3390/nu15081929, PMID 37111148 In: https://www. mdpi. com/2072-6643/15/8/1929.
22. Akanda MK, Hasan AH, Mehjabin S, Parvez GM, Yasmin S, Akhtar MS et al. *Carica papaya* in health and disease: a review of its bioactive compounds for treating various disease conditions, including anti-inflammatory and anti-arthritic activities. Inflammopharmacology. 2025 Jun 20;33(6):3051-84. doi: 10.1007/s10787-025-01780-4, PMID 40392387.
23. Nayak SB, Pinto Pereira LP, Maharaj D. Wound healing activity of *Carica papaya* L. in experimentally induced diabetic rats. Indian J Exp Biol. 2007;45(8):739-43. PMID 17877152.

24. Manosroi A, Chankhampan C, Manosroi W, Manosroi J. Transdermal absorption enhancement of papain loaded in elastic niosomes incorporated in gel for scar treatment. Eur J Pharm Sci. 2013;48(3):474-83. doi: 10.1016/j.ejps.2012.12.010, PMID 23266464.
25. Altinkaynak C, Haciosmanoglu E, Ekremoglu M, Hacioglu M, Özdemir N. Anti-microbial, anti-oxidant and wound healing capabilities of *Aloe vera*-incorporated hybrid nanoflowers. J Biosci Bioeng. 2023;135(4):321-30. doi: 10.1016/j.jbiosc.2023.01.004, PMID 36806412.
26. Jettanacheawchankit S, Sasithanasate S, Sangvanich P, Banlunara W, Thunyakitpisal P. Acemannan stimulates gingival fibroblast proliferation; expressions of keratinocyte growth factor-1, vascular endothelial growth factor, and type I collagen; and wound healing. J Pharmacol Sci. 2009;109(4):525-31. doi: 10.1254/jphs.08204FP, PMID 19372635.
27. Bhalang K, Thunyakitpisal P, Rungsirisatean N. Acemannan, a polysaccharide extracted from *Aloe vera*, is effective in the treatment of oral aphthous ulceration. J Altern Complement Med. 2013;19(5):429-34. doi: 10.1089/acm.2012.0164, PMID 23240939.
28. Kumar A, Kalia AN, Singh H. Standardization of optimized anti-diabetic polyherbal formulation by HPLC. Int J Pharm Sci Drug Res. 2021 Mar 30:158-63. doi: 10.25004/IJPSDR.2021.130207/index. php/journal/article/view/2106.
29. Nalimu F, Oloro J, Peter EL, Ogwang PE. Acute and sub-acute oral toxicity of aqueous whole leaf and green rind extracts of *Aloe vera* in Wistar rats. BMC Complement Med Ther. BioMed Central. 2022 Dec 14;22(1):16. doi: 10.1186/s12906-021-03470-4, PMID 35031035.
30. Chelu M, Musuc AM, Popa M, Calderon Moreno J. *Aloe vera*-based hydrogels for wound healing: properties and therapeutic effects. Gels. 2023 Jul 3;9(7):539. doi: 10.3390/gels9070539, PMID 37504418 In: https://www. mdpi. Com/2310-2861/9/7/539.
31. Vozza G, Danish M, Byrne HJ, Frías JM, Ryan SM. Application of Box-Behnken experimental design for the formulation and optimisation of selenomethionine-loaded chitosan nanoparticles coated with zein for oral delivery. Int J Pharm. 2018;551(1-2):257-69. doi: 10.1016/j.ijpharm.2018.08.050, PMID 30153488.
32. Mahmoud BS, McConville C. Formulation and systematic optimisation of polymeric blend nanoparticles via Box–Behnken design. Pharmaceutics. 2025 Oct 20;17(10):1351. doi: 10.3390/pharmaceutics17101351, PMID 41155986 In: https://www. mdpi. com/1999-4923/17/10/1351.
33. Rathee S, Kamboj A. Optimization and development of antidiabetic phytosomes by the Box–Behnken design. J Liposome Res. 2018 Apr 3;28(2):161-72. doi: 10.1080/08982104.2017.1311913, PMID 28337938 In: https://www. tandfonline. com/doi/full/10.1080/08982104.2017.1311913.
34. Mariam Joshua J, Anilkumar A, Cu V, T Vasudevan D, A Surendran S. Formulation and evaluation of antiaging phytosomal gel. Asian J Pharm Clin Res. 2018 Mar 1;11(3):409. doi: 10.22159/ajpcr.2018.v11i3.24257. in/journals/index. php/ajpcr/article/view/24257.
35. D.R, M.N, V. J, P.P. development, characterization and evaluation of phytosomal gel of curcumin for the treatment of topical fungal infection. Int J Newgen Res Pharm Healthc. 2023 Jun 30:62-9. Available In: https://www. ijnrph. com/index. php/ijnrph/article/view/16.
36. Wanjiru J, Gathirwa J, Sauli E, Swai HS. Formulation, optimization, and evaluation of *Moringa oleifera* Leaf polyphenol-loaded phytosome delivery system against breast cancer cell Lines. Molecules. 2022 Jul 11;27(14):4430. doi: 10.3390/molecules27144430, PMID 35889305 In: https://www. mdpi. Com. 1420-3049/27/14/4430.
37. Chen X, Fan X, Li F. Development and evaluation of a novel diammonium glycyrrhizinate phytosome for nasal vaccination. Pharmaceutics. 2022 Sep 21;14(10):2000. doi: 10.3390/pharmaceutics14102000, PMID 36297436 In: https://www. mdpi. com/1999-4923/14/10/2000.
38. Chen X, Yu S, Wang P, Zhao X, Sang G. Development and evaluation of a novel hyaluronic acid and chitosan-modified phytosome for co-delivery of oxymatrine and glycyrrhizin for combination therapy. Recent Pat Anticanc Drug Discov [Internet]. 2024 May;19(2):154-64. doi: 10.2174/1574892818666230215112942, PMID 38214355 In: https://www. eurekaselect. com/213693/article.
39. Chittasupho C, Chaobankrang K, Sarawungkad A, Samee W, Singh S, Hemsuwimon K et al. Antioxidant, anti-inflammatory and attenuating intracellular reactive oxygen species activities of *Nicotiana tabacum* var. Virginia Leaf extract phytosomes and shape memory gel formulation. Gels. 2023 Jan 18;9(2):78. doi: 10.3390/gels9020078, PMID 36826248 In: https://www. mdpi. Com/2310-2861/9/2/78.
40. Jain P, Taleuzzaman M, Kala C, Kumar Gupta D, Ali A, Aslam M. Quality by design (Qbd) assisted development of phytosomal gel of *Aloe vera* extract for topical delivery. J Liposome Res. 2021 Oct 2;31(4):381-8. doi: 10.1080/08982104.2020.1849279, PMID 33183121 In: https://www. tandfonline. com/doi/full/10.1080/08982104.2020.1849279.
41. Anwar E, Farhana N. Formulation and evaluation of phytosome-loaded maltodextrin-gum arabic microsphere system for delivery of *Camellia sinensis* extract. J Young Pharm. 2018;10(2s):S56-62. doi: 10.5530/jyp.2018.2s.11.
42. Sohal JK, Saraf A, Shukla KK, Shrivastava M. Determination of antioxidant potential of biochemically synthesized silver nanoparticles using *Aloe vera* gel extract. Plant Sci Today. 2019;6(2):208-17. doi: 10.14719/pst.2019.6.2.532.
43. Zhao P, Ming Q, Qiu J, Tian D, Liu J, Shen J et al. Ethanolic extract of folium Sennae mediates the glucose uptake of L6 cells by GLUT4 and Ca2. Molecules. 2018;23(11):2934. doi: 10.3390/molecules23112934, PMID 30424024.
44. Pulivarthi V, Josthna P, Naidu CV. *In vitro* antidiabetic activity by glucose uptake of yeast cell assay and antioxidant potential of *Annona reticulata l*. Int J Pharm Sci Drug Res. 2020:208-13. doi: 10.25004/IJPSDR.2020.120301.
45. SSP, BHAT MP, NAYAKA S. Microbial synthesis of silver nanoparticles using *Streptomyces sp* and their characterization, antimicrobial activity, and cytotoxicity assessment against human lung (a549) and breast (Mcf-7) cancer cell Lines. Int J Pharm Pharm Sci. 2021;13(8):94-102.
46. Kumar KN, Devarajan N, Amritkumar P, Munusamy T, Suresh M, S MB. Green synthesis of chitosan-mediated silver nanocomposite using *Piper betel* stem extract: evaluating antibacterial and anticancer activity. Vol. 19(1); 2026.
47. Gore DD, Mishra N, Kumar D, Jena G, Jachak SM, Tikoo K et al. Anti-inflammatory activity, stability, bioavailability and toxicity studies on seabuckthorn polyphenol enriched fraction and its phospholipid complex (Phytosomes) preparation. Int J Biol Macromol. 2025 Mar;297:139919. doi: 10.1016/j.ijbiomac.2025.139919, PMID 39824425.
48. Kant V, Gopal A, Pathak NN, Kumar P, Tandan SK, Kumar D. Antioxidant and anti-inflammatory potential of curcumin accelerated the cutaneous wound healing in streptozotocin-induced diabetic rats. Int Immunopharmacol. 2014;20(2):322-30. doi: 10.1016/j.intimp.2014.03.009, PMID 24675438.
49. Lodhi S, Singhai AK. Preliminary pharmacological evaluation of *Martynia annua* Linn leaves for wound healing. Asian Pac J Trop Biomed. ScienceDirect. 2011;1(6):421-7. doi: 10.1016/S2221-1691(11)60093-2.
50. Hashemnia M, Nikousefat Z, Mohammadalipour A, Zangeneh MM, Zangeneh A. Wound healing activity of *Pimpinella anisum* methanolic extract in streptozotocin-induced diabetic rats. J Wound Care. 2019;28(10) Sup10:S26-36. doi: 10.12968/jowc.2019.28.Sup10.S26, PMID 31600102.
51. Gür R, Büyükakyüz N, Aydil BA, Ayhan M. Deneysel olarak oluşturulmuş diyabetik sıçanlarda kitosanın oral mukozada yara iyileşmesine etkisinin histopatolojik araştırılması [Histopathological investigation of the effect of chitosan on oral mucous wound healing in experimentally established diabetic rats]. Ulus Travma Acil Cerrahi Derg. 2023;29(2):140-8. doi: 10.14744/tjtes.2022.55726, PMID 36748767.